2011

THE CONSEQUENCE OF ODDD HYPOMYELINATION-LINKED Cx43 MUTATIONS ON HETEROTYPIC GAP JUNCTIONAL INTERCELLULAR COMMUNICATION BETWEEN Cx43/Cx47 GAP JUNCTION CHANNELS

Andrew MacDonald

THE CONSEQUENCE OF ODDD HYPOMYELINATION-LINKED Cx43 MUTATIONS ON HETEROTYPIC GAP JUNCTIONAL INTERCELLULAR COMMUNICATION BETWEEN Cx43/Cx47 GAP JUNCTION CHANNELS

(Spine Title: Cx43 Mutations in Central Hypomyelination)

(Thesis Format: Monograph)

By

Andrew MacDonald
Graduate program in Physiology and Pharmacology

A thesis submitted in partial fulfillment
Of the requirements for the degree of
Master of Science

The School of Graduate and Postdoctoral Studies
The University of Western Ontario
London, Ontario, Canada

THE UNIVERSITY OF WESTERN ONTARIO
SCHOOL OF GRADUATE AND POSTGRADUATE STUDIES

CERTIFICATE OF EXAMINATION

Supervisor

Dr. Donglin Bai

Supervisory Committee

Dr. Barry Tepperman

Dr. Stephen Karlik

Dr. Dan Belliveau

Examiners

Dr. Arthur Brown

Dr. Wei-Yang Lu

Dr. Susanne Schmid

The thesis by

Andrew MacDonald

Entitled:

THE CONSEQUENCE OF ODDD HYPOMYELINATION-LINKED Cx43 MUTATIONS ON HETEROTYPIC GAP JUNCTIONAL INTERCELLULAR COMMUNICATION BETWEEN Cx43/Cx47 GAP JUNCTION CHANNELS

Is accepted in partial fulfillment of the

Requirements for the degree of

Master of Science

Date_____

Chair of Thesis Examination Board

Abstract

Gap junction (GJ) channels, a conduit for intercellular communication between adjacent cells, are composed of connexins (Cxs). Human macroglial cells express non-overlapping Cxs with oligodendrocytes expressing Cx47, Cx32 and Cx29 while astrocytes express Cx43, Cx30 and Cx26. Intercellular communication between oligodendrocytes and astrocytes depends on heterotypic GJ channels, predominantly Cx47/Cx43 heterotypic channels. Mutations in either Cx47 or Cx43 have been linked to central hypomyelination diseases, suggesting a critical role of Cx47/Cx43 GJ channels. Moreover, patients with Cx43 mutations exhibit pleiotropic phenotypes with only some mutations linking to central hypomyelination. Our aim is to study functional changes of hypomyelination-linked Cx43 mutants K134N, G138R, and V96A against non-hypomyelination-linked Cx43 mutants R76H, H194P, and V96M. We found that all mutants were functionally impaired in either homotypic or heterotypic GJ channel formation with Cx47, suggesting that electrical coupling via the heterotypic Cx43/Cx47 GJ channels may not be critical in the maintenance of central myelination.

Keywords: central nervous system, connexins, gap junctions, gap junctional intercellular communication, hypomyelination, oculodentodigital dysplasia, Pelizaeus Merzbacher-like disease.

Dedication

For Mom and Dad

Acknowledgements

First, I would like to recognize my supervisor Dr. Donglin Bai for the opportunity to develop my knowledge on the basic processes of science. His guidance in the scientific process and his expertise on electrophysiological methods allowed me to grow as a researcher and a student. Most of all I would like to thank him for his never ending patience. Any student would be lucky to have Dr. Bai as a scientific mentor and friend; he truly made my time enjoyable. Second, I would like to thank the entire Bai laboratory, especially Dr. Xiang Qun Gong and Li Xin for their gracious advice in numerous laboratory techniques and technical support. It was their hands on advice which allowed my project to flow smoothly from start to finish. I wish you all the best in your future endeavours and scientific careers. Finally, I would like thank my parents. Their never ending moral support provided me with the motivation to and focus needed to pursue my academic career. Words will never be able to express how much you both have done for me.

Table of Contents

List of Figures

List of Tables

List of abbreviations and nomenclature

ATCC	american type culture collection
ATP	adenosine tri-phosphate
A/A	astrocyte/astrocyte coupling
A/O	astrocyte/oligodendrocyte coupling
BBB	blood brain barrier
cDNA	complementary deoxyribonucleic acid
CL	intracellular loop
CNS	central nervous system
CT	carboxyl terminal
Cx	connexin
DAPI	4',6-diamidino-2-phenylindole
DMEM	dulbecco's modified eagle medium
E1	first extracellular loop
E2	second extracellular loop
ER	endoplasmic reticulum
G_j	macroscopic gap junctional conductance
GFP	green fluorescent protein
GJ	gap junction
GJIC	gap junctional intercellular communication
HeLa	cervical cancer cell line
I_j	transjunctional current
kDa	kilo-dalton

LY	lucifer yellow
MRI	magnetic resonance imaging
N2A	neuroblastoma cell line
NT	amino terminal
O/O	oligodendrocyte/oligodendrocyte coupling
ODDD	oculodentodigital dysplasia
PLP1	proteolipid protein-1
PMD	pelizaeus merzbacher disease
PMLD	pelizaeus merzbacher-like disease
RFP	red fluorescent protein
V_j –gating	transjunctional voltage dependent gating
WPI	world precision instruments
WT	wild-type

1.0 Literature Review

1.1 Introduction

Individual cells are the basic functional units of life and are unique in terms of their dynamic metabolisms, growth properties, and susceptibilities to protective and deat5h promoting signals. Cells also have varying migratory capabilities, and are able to adhere to other cells of similar or different types. Multi-cellular organisms contain hundreds to trillions of cells all acting in concert for the overall development, growth and proliferation of the organism. In order to do this, cells must be able to effectively communicate with one another and thus, the entire multi-cellular system is dependent on the presence of a complex, yet precise means of intercellular communication. Intercellular communication can occur through indirect or direct mechanisms, whereby direct intercellular communication occurs via gap junction (GJ) channels, which is termed gap junctional intercellular communication (GJIC) (Furshpan and Potter 1957; Gilula 1987). GJIC provides multi-cellular organisms with a means for individual cells to regulate metabolism, growth, proliferation and apoptosis (Maeda and Tsukihara 2011). Experimental data illustrates that disruption of GJIC in animals can result in various abnormalities regarding these specific processes (Paznekas, Boyadjiev et al. 2003). Specifically, a dominant murine connexin43 (Cx43) mutation G60S, was identified by an N-ethyl-N-nitrosourea mutagenesis screen and was shown to cause a phenotype similar to the human disease Oculodentodigital dysplasia (ODDD). This particular mutation causes alterations in Cx43 expression, GJIC, and the overall phenotype (Flenniken, Osborne et al. 2005; Xin, Gong et al. 2011).

1.2 Gap Junction Structure

Gap junction structure was first defined in 1967 by Revel and Karnovsky. Using electron microscopy on preparations of heart and liver tissue Revel and Karnovsky indentified regions of the plasma membrane where two closely apposed cells were separated by a consistent 2-3 nm gap (Revel and Karnovsky 1967). It was later discovered that these "gap" junctional areas consisted of tens to thousands of GJ channels (Chalcroft and Bullivant 1970; Goodenough and Revel 1970). A recent crystal structure study at a 3.5 angstrom resolution on human Cx26 predicts that the gap formed between two cells is 3-4nm (Maeda, Nakagawa et al. 2009). It has long been known that cell pairs are coupled via intercellular mechanisms. Functional studies using microelectrodes provided evidence of electrical synapses directly coupling two cells, which was later found to be a conduit consisting of GJ channels (Furshpan and Potter 1959; Gong, Shao et al. 2007).

1.3 Connexins

Connexins constitute a highly conserved family of integral membrane proteins that serve as the building blocks for connexons (Goodenough, Goliger et al. 1996). There are 21 human and 20 murine Cx isoforms which are named according to their calculated molecular weight, ranging between 26 to 57 kilo-Daltons (kDa) (Willecke, Eiberger et al. 2002). Connexin topology consists of four transmembrane domains (M1-M4), intracellular carboxyl and amino terminals (CT and NT), one cytoplasmic loop (CL), and two extracellular loops designated as E1 and E2 (Figure 1-1) (Goodenough and Revel 1970; Maeda, Nakagawa et al. 2009). Connexins are

differentially expressed in various cell and tissue types. For instance, Cx43 is expressed in an extensive number of tissue types throughout the human body, where as Cx47 is primarily localized to lymphatic endothelial cells and oligodendrocytes in the CNS (Menichella, Goodenough et al. 2003; Li, Ionescu et al. 2004; Orthmann-Murphy, Enriquez et al. 2007; Ferrell, Baty et al. 2010).

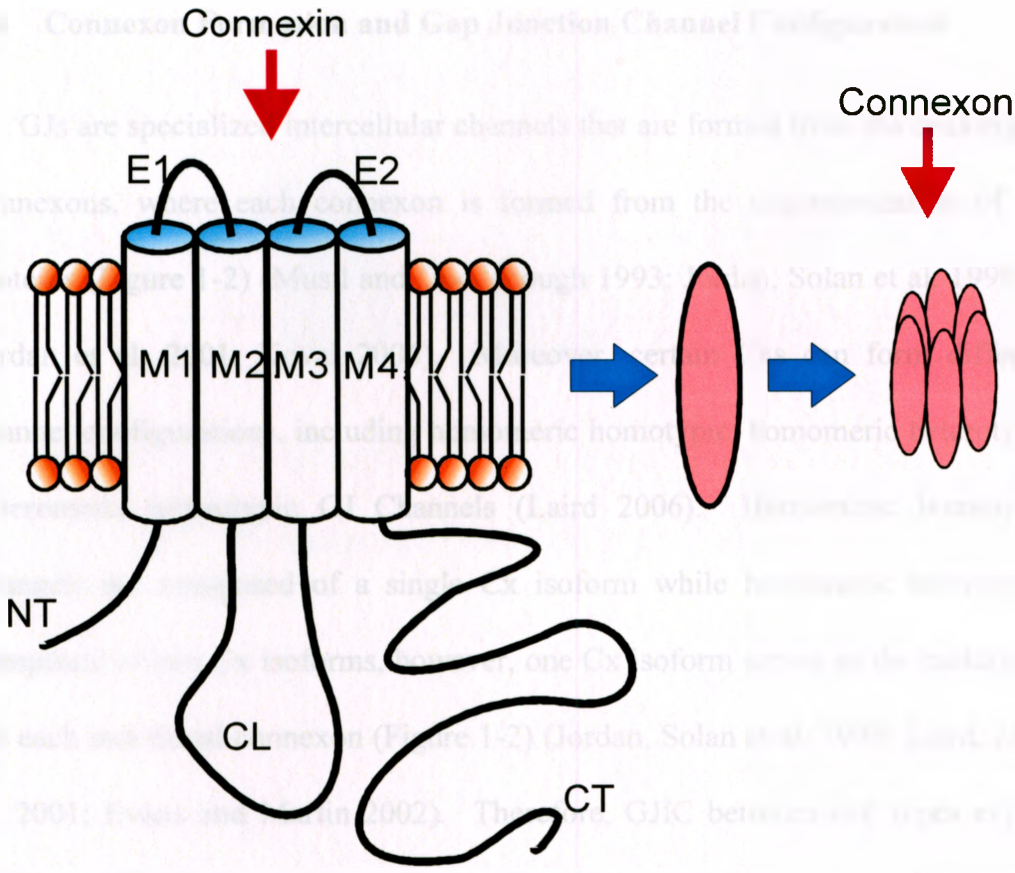

Figure 1-1: Schematic diagram of Cx topology and connexon. All Cxs are predicted to share a similar topology with four transmembrane domains (M1-M4), intracellular amino- (NT) and carboxyl- (CT) termini, one intracellular loop (CL), and two extracellular loops designated as E1 and E2. Individual Cxs oligomerize into hexameric protein structures known as connexons.

1.4 Connexon Formation and Gap Junction Channel Configuration

GJs are specialized intercellular channels that are formed from the docking of two connexons, where each connexon is formed from the oligomerization of six Cx proteins (Figure 1-2) (Musil and Goodenough 1993; Jordan, Solan et al. 1999; Laird, Jordan et al. 2001; Koval 2006). Moreover, certain Cxs can form different GJ channel configurations, including homomeric homotypic, homomeric heterotypic and heteromeric heterotypic GJ Channels (Laird 2006). Homomeric homotypic GJ channels are composed of a single Cx isoform while homomeric heterotypic are composed of two Cx isoforms, however, one Cx isoform serves as the building block for each individual connexon (Figure 1-2) (Jordan, Solan et al. 1999; Laird, Jordan et al. 2001; Evans and Martin 2002). Therefore, GJIC between cell types expressing different Cx isoforms must be mediated through homomeric heterotypic or heteromeric heterotypic GJ channels. For my studies I focus on either homomeric homotypic or homomeric heterotypic GJ channels.

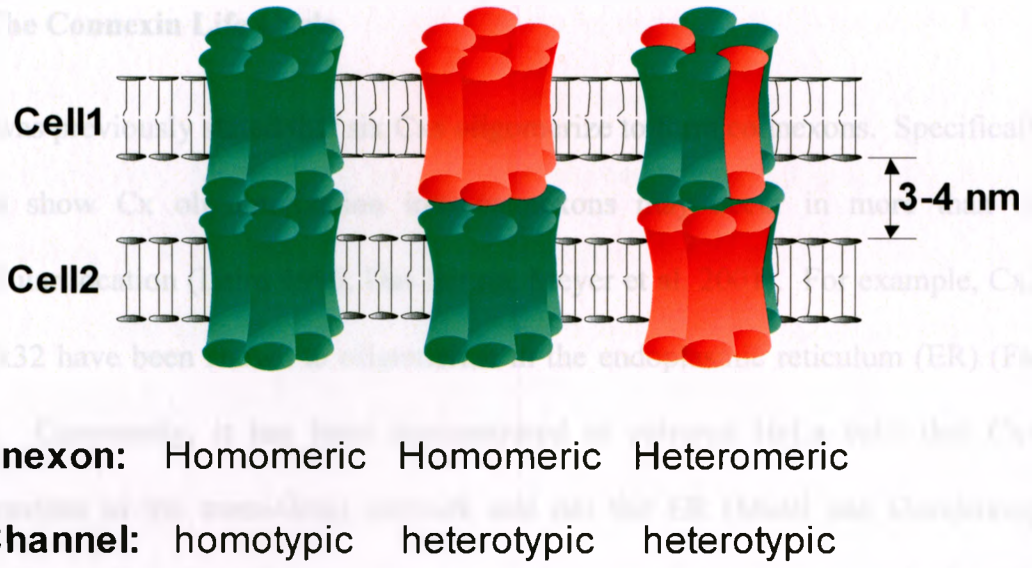

Figure 1-2: Connexon and gap junction (GJ) configurations. Connexons may be composed of a single Cx type designated as homomeric, or of two Cx types, designated as heteromeric. GJ channels composed of two like connexons are designated as homotypic GJ channels, while GJ channels composed of dissimilar connexons are designated as heterotypic GJ channels. The extracellular region is approximately 3-4 nm in length.

1.5 The Connexin Life Cycle

It was previously stated that six Cxs oligomerize to form connexons. Specifically, studies show Cx oligomerization into connexons may occur in more than one subcellular location (Laird 1996; Das Sarma, Meyer et al. 2001). For example, Cx26 and Cx32 have been shown to oligomerize in the endoplasmic reticulum (ER) (Falk 2000). Conversely, it has been demonstrated in cultured HeLa cells that Cx43 oligomerizes in the trans-Golgi network and not the ER (Musil and Goodenough 1993). Generally, after oligomerization, a vesicle containing connexons buds off of the trans-Golgi network and is carried to the cell membrane via the microtubule network (Thomas, Jordan et al. 2005; Laird 2006). Finally, once connexons are present in the cell membrane, they diffuse laterally within the cell surface and can dock with compatible connexons in closely apposed cells (Falk 2000; Thomas, Jordan et al. 2005). When compatible connexons dock the result is the formation of GJ channels denoted by the presence of GJ plaque-like structures (Thomas, Jordan et al. 2005). GJ channels are dynamic structures that are continuously undergoing assembly, internalization and degradation. Furthermore, the mean half-life of GJ channels ranges between 3-5 hours (Laird 1996; Laird 2006). This quick turnover allows individual cells to up- or down- regulate GJ channels, effectively mediating GJIC between two cells (Lauf, Giepmans et al. 2002; Laird 2006).

GJ internalization occurs via an endocytic pathway, and new channels can replace the endocytosed GJs via lateral diffusion (Laird 1996). Moreover, internalized GJ junction channels are termed annular GJs or "connexosomes", and have been visualized as double-membrane intracellular structures (Laird, Jordan et al. 2001).

Research has demonstrated that annular GJs can be degraded by either a proteosomal or lysosomal pathway (Sasaki and Garant 1986; Severs, Shovel et al. 1989; Leithe and Rivedal 2004). Moreover, it has also been shown that ubiquitinated GJs from the ER, including those composed of Cx43, were targeted for degradation (Laird, Jordan et al. 2001; Leithe and Rivedal 2004). Overall, a multitude of data suggests that Cxs are highly regulated within individual cells.

Figure 1-3: Schematic diagram of the Cx life cycle. Cxs are synthesized in the endoplasmic reticulum (ER) and oligomerize into connexons in either the ER or trans-Golgi network. Connexons are then trafficked along the microtubule network to the plasma membrane, where they are inserted as a closed channel. Furthermore, connexons laterally diffuse through the plasma membrane and dock with compatible connexons on an apposing cell membrane, creating GJ plaques. GJ plaques are internalized through an endocytic pathway, and will then undergo degradation via a lysosomal or proteosomal pathway.

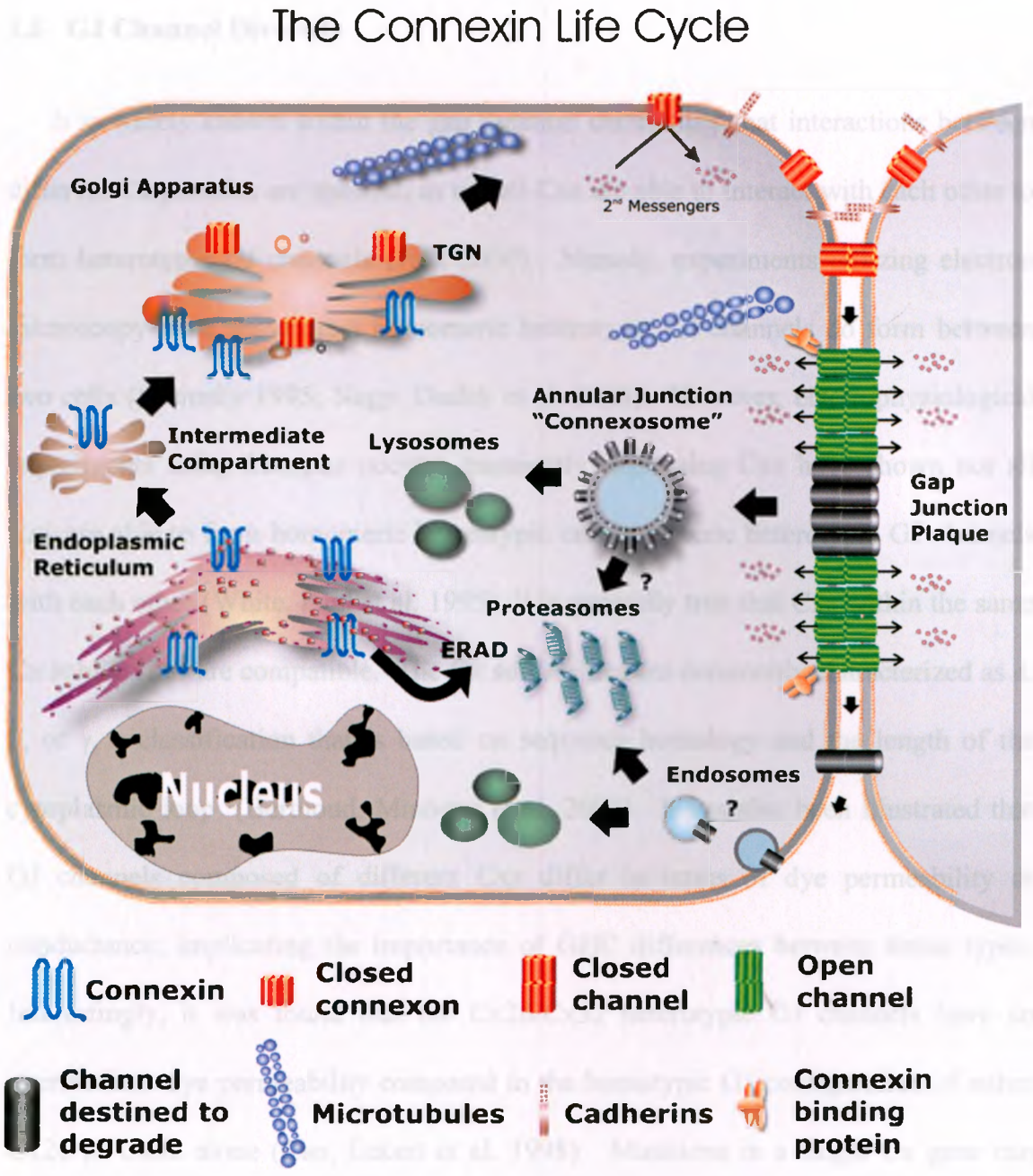

Figure 1-3 (Adapted from Laird et al., 2006)

1.6 GJ Channel Diversity

It is widely known within the gap junction community that interactions between different Cx proteins are specific, as not all Cxs are able to interact with each other to form heterotypic GJ channels (Falk 2000). Namely, experiments utilizing electron microscopy have shown that homomeric heterotypic GJ channels do form between two cells (Sosinsky 1995; Nagy, Dudek et al. 2004). However, electrophysiological experiments using *Xenopus* oocytes transiently expressing Cxs have shown not all Cxs are able to form homomeric heterotypic or heteromeric heterotypic GJ channels with each other (White, Paul et al. 1995). It is generally true that Cxs within the same Cx subfamilies are compatible. The Cx subfamilies are commonly characterized as α, β, or γ, a classification that is based on sequence homology and the length of the cytoplasmic loop (Berthoud, Minogue et al. 2004). It has also been illustrated that GJ channels composed of different Cxs differ in terms of dye permeability or conductance, implicating the importance of GJIC differences between tissue types. Interestingly, it was found that the Cx26/Cx32 heterotypic GJ channels have an intermediate dye permeability compared to the homotypic GJ configuration of either Cx26 or Cx32 alone (Cao, Eckert et al. 1998). Mutations in a single Cx gene can affect the function of GJ channels, altering GJIC between cells, and can be detrimental to the function of a multi-cellular organism (Orthmann-Murphy, Salsano et al. 2009; Paznekas, Karczeski et al. 2009). For example, mutations in either Cx43 or Cx47 can alter GJ expression, resulting in central nervous system (CNS) hypomyelination (Paznekas, Boyadjiev et al. 2003; Orthmann-Murphy, Enriquez et al. 2007).

1.7 Gap Junction Coupling

GJs allow direct electric coupling between the cytoplasm's of two cells and also allow passage of small molecules up to 1 kDa in size (Evans and Martin 2002; Orthmann-Murphy, Abrams et al. 2008). Interestingly, experimental data has shown that different Cx isoforms will have an altered ability to pass dyes, depending on the size and charge of the dye. Specifically, studies in HeLa cells have shown that Cx26, Cx32, and Cx45 transfer lucifer yellow (LY) (anionic 457 Da) dye, and 4',6-diamidino-2-phenylindole (DAPI) (cationic 350 Da) with different kinetics and permeability (Cao, Eckert et al. 1998; Rackauskas, Verselis et al. 2007). In particular, Cx32 coupled *Xenopus* oocytes were six times more permeable to LY than Cx26 coupled ooctyes (Cao, Eckert et al. 1998). Thus, it is evident that dye permeability varies between different types of GJ channels and that this difference can be experimentally determined. Nonetheless, dye transfer assay is a crude qualitative way of analyzing of gap junction coupling.

The dual whole-cell patch clamp technique is a much more sensitive method than dye transfer assays when determining the degree of gap junction coupling where macroscopic junctional conductance (G_j) between two gap junction coupled cells can be measured directly(Neher, Sakmann et al. 1978). For example, minute differences in single channel conductance (pico Siemens range) can be detected between two cells (Rook, Jongsma et al. 1988). The dual whole-cell patch clamp technique is an invaluable tool to precisely measure gap junctional coupling or specifically, G_j. For example, the dual whole-cell patch clamp technique is able to distinguish GJs based upon their individual voltage dependent gating properties, which is the closure of GJ

channels in response to voltage changes (Bukauskas, Bukauskiene et al. 2001; Rackauskas, Kreuzberg et al. 2007).

1.8 Connexin Expression in Macroglia

Central nervous system (CNS) macroglial cells describe two non-neuronal cell types important to CNS function, astrocytes and oligodendrocytes. Astrocytes aid in the formation of the blood brain barrier (BBB) and may be important in the spatial buffering of potassium after prolonged neuronal activity (Kamasawa, Sik et al. 2005). Oligodendrocytes form myelin around specific CNS axons and serve as an insulating sheath (myelin sheath) to ensure a rapid propagation of action potentials (Orthmann-Murphy, Abrams et al. 2008). Astrocytes and oligodendrocytes have specific Cx expression profiles (Orthmann-Murphy, Abrams et al. 2008). Astrocytes express three Cx isoforms, Cx43, Cx30, and Cx26 (Kunzelmann, Schroder et al. 1999; Nagy, Li et al. 2001; Rash, Yasumura et al. 2001; Rouach, Avignone et al. 2002; Nagy, Ionescu et al. 2003) while, oligodendrocytes express Cx47, Cx32, and Cx29 (Altevogt, Kleopa et al. 2002; Odermatt, Wellershaus et al. 2003; Menichella, Majdan et al. 2006). Astrocytes and oligodendrocytes are extensively interconnected with one another and to themselves through GJ channels (Maglione, Tress et al. 2010; Magnotti, Goodenough et al. 2010; Wasseff and Scherer 2011).

1.9 Cx47 and Peliazeus Merzbacher-like Disease

Pelizaeus Merzbacher-like Disease (PMLD) is a rare genetic disorder caused by recessive mutations in the gene encoding Cx47, known as GJC2 (Orthmann-Murphy, Enriquez et al. 2007). A similarly termed disease, Pelizaeus Merzbacher Disease

(PMD), an X-linked demyelinating disorder is caused by mutations in *Proteolipid Protein 1* (PLP1), which is a vital membrane protein of CNS myelin. The clinical phenotype of both PMD and PMLD is commonly described by nystagmus, ataxia, progressive spasticity, and developmental delays (Uhlenberg, Schuelke et al. 2004). Magnetic resosance imaging (MRI) of PMLD patients also reports severe CNS demyelination (Orthmann-Murphy, Salsano et al. 2009). Conversely, CNS myelination of *Cx47*-null mice is not signifcantly affected and mice show no overt pathological phenotypic differences (Odermatt, Wellershaus et al. 2003). Nonetheless, this may be attributed by the differences between murine and human glial physiology. It is thus interesting that only certain mutations in *Cx47* cause severe demyeliantion in the CNS. Thus, it has been suggested that Cx mutations associated with PMLD will cause a disruption of astrocyte/oligodendrocyte coupling (A/O) coupling, mediated mainly via the Cx43/Cx47 heterotypic GJ channel (Orthmann-Murphy, Enriquez et al. 2007).

Specific Cx47 proteins harbouring mutations appear to be intracellularly retained and unable to reach cell surface to form functional GJ channels. For example, three particular missense *Cx47* mutations associated with PMLD, Cx47P87S, Cx47Y269D and Cx47M283T were chosen to assess the trafficking (Orthmann-Murphy, Freidin et al. 2007). It was found that wild-type (WT) Cx47 was able to form GJ plaques while the three PMLD associated Cx47 mutants were unable to traffic to the cell surface in HeLa and N2A cells (Orthmann-Murphy, Enriquez et al. 2007). In the same study it was discovered that WT Cx47 GJ channels were functional GJ channels in N2A cells, while *Cx47* mutations, Cx47P87S, Cx47Y269D, and Cx47M283T were completely

non-functional in both homotypic configurations or with WT Cx47 (Orthmann-Murphy, Enriquez et al. 2007).

More recent studies show that there are less detrimental *Cx47* mutations including the I33M mutation, which has been described as causing a milder neurological phenotype when compared against PMLD-associated *Cx47* mutations (Orthmann-Murphy, Salsano et al. 2009). I33M mutant cDNA was generated and inserted into a pIRES2-EGFP vector for assessment via dual-whole cell patch recording. Results show that the I33M mutant was not functional as a homotypic GJ channel, paired with WT Cx47, or with WT Cx43. However, in the same study immunofluorescent assays illustrate that this mutant was able to traffic to the cell membrane and form plaques similar to those of WT Cx47 in HeLa cells (Orthmann-Murphy, Salsano et al. 2009). There are numerous reported *Cx47* mutations whose trafficking and function remain to be studied, and not all *Cx47* mutations result in non-functional homotypic GJ channels (Kim et al., unpublished data).

1.10 Cx43 and Oculodentodigital Dysplasia

Oculodentodigital dysplasia is a rare genetic disorder, attributable to more than seventy different mutations in *Cx43*. ODDD patients display a pleiotropic phenotype with a variety of symptoms, including, micropthalmia, microcornea, enamel hypoplasia, syndactly, campodactly, and neurological manifestations (Paznekas, Karczeski et al. 2009). Interestingly, only a subset of ODDD patients develop severe neurological manifestations, specifically CNS demyelination. It is unclear why only certain *Cx43* mutations cause CNS hypomyelination and others do not. It is the goal

of this current study to investigate the presence of any unique defects associated with CNS hypomyelination-linked Cx43 mutants.

The ability of hypomyelination-linked ODDD *Cx43* mutants to form functional homotypic or heterotypic GJ channels with Cx47 is not fully characterized. In response, we have selected two subsets of ODDD *Cx43* mutants for this study, one set that is linked to CNS hypomyelination and one that is not. The various ODDD CNS hypomyelination-linked and CNS non-hypomyelination-linked Cx43 mutants are shown schematically in Figure 1-4. The *Cx43* mutants linked to CNS hypomyelination are K134N, G138R, and V96A and those that are not linked to CNS hypomyelination are R76H, V96M, and H194P (Gladwin, Donnai et al. 1997; Paznekas, Boyadjiev et al. 2003; Kjaer, Hansen et al. 2004; Pizzuti, Flex et al. 2004; Vitiello, D'Adamo et al. 2005; Paznekas, Karczeski et al. 2009). By analyzing the ability of the *Cx43* mutants in each set to form heterotypic GJ channels with Cx47, we can elucidate the importance of the Cx43/C47 heterotypic GJ channel and its role in CNS myelination.

1.11 Astrocyte/Oligodendrocyte Coupling

It is known that astrocytes and oligodendrocytes express different Cx subsets, Cx26, Cx30, and Cx43, or Cx29, Cx32, and Cx47, respectively. However, it is thought that Cx26 and Cx29 do not significantly contribute to the formation of GJ channels (Altevogt, Kleopa et al. 2002; Maglione, Tress et al. 2010). Both anatomical and functional studies of mice and rats have illustrated that astrocytes and oligodendrocytes are coupled by gap junction channels (Nagy, Ionescu et al. 2003;

Odermatt, Wellershaus et al. 2003). Moreover, dual-whole cell patch clamping studies on N2A cells have elucidated possible heterotypic configurations that can be formed between astrocyte/oligodendrocyte cell pairs (A/O). Cx43/Cx47 and Cx30/Cx32 heterotypic pairings are able to dock and form functional GJ channels while Cx43/Cx32, Cx30/Cx47 heterotypic pairings were not found to be functional as determined by confocal imaging and dual whole-cell recordings, respectively. (Orthmann-Murphy, Abrams et al. 2008). The contribution of Cx26/Cx32 and Cx26/Cx47 heterotypic GJ channels remained uncertain. Studies using both immunolabelling and electron microscopy have revealed that Cx43/Cx47 channels outnumber Cx30/Cx32 channels at oligodendroglial cell bodies (Kamasawa, Sik et al. 2005). Nonetheless, electrophysiological techniques used to assess dye transfer between oligodendrocyte/oligodendrocyte (O/O), astrocyte/astrocyte (A/A), and A/O in tissue sections illustrates some key differences when compared against the in vitro studies. Specifically, it has been discovered that Cx30/Cx47 and Cx47/Cx47 channels are able to pass the GJ permeable dye biocytin (Maglione, Tress et al. 2010; Wasseff and Scherer 2011).

It is widely known that both Cx32/Cx30 and Cx47/Cx43 GJ channels couple astrocytes to oligodendrocytes, however, it is thought that Cx47/Cx43 GJs are more specific to this role. In Cx32-null mice it has been shown that A/O coupling is unaffected in the neocortex (Wasseff and Scherer 2011). Additionally, mutations in *Cx32* cause Charcot-Marie-Tooth disease (CMTX1), an X-linked demyelinating neuropathy (Scherer, Xu et al. 1998). However, CMTX1 patients typically do not have CNS dysfunction which indicates that Cx32/Cx30 GJ channels are not of critical

importance in humans (Orthmann-Murphy, Abrams et al. 2008). Thus, it is believed that the Cx43/Cx47 heterotypic GJ channel forms the primary GJ channel between oligodendrocytes and astrocytes. A/O Cx compatibility is demonstrated graphically in Figure 1-5.

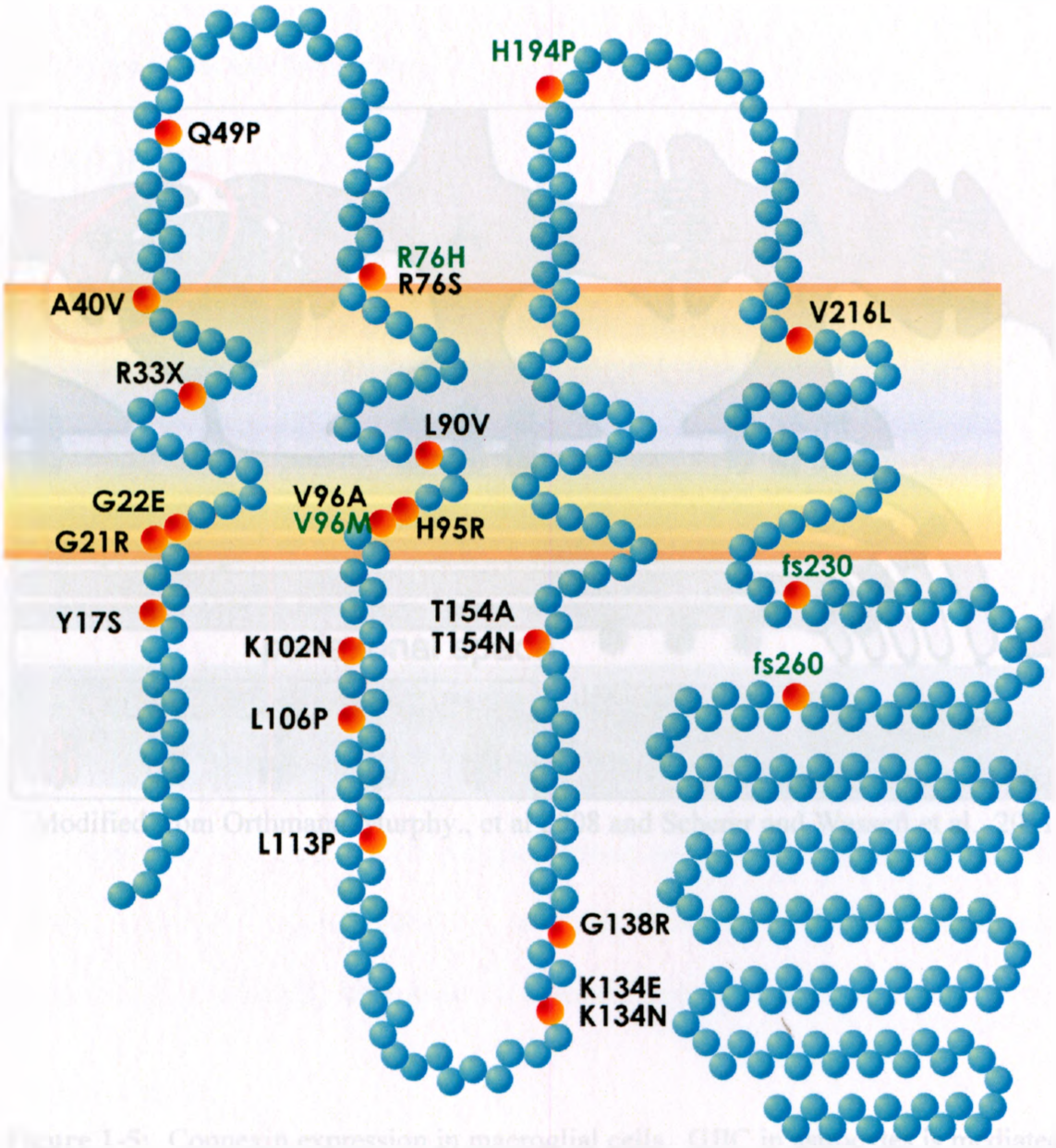

Figure 1-4: Cx43 topology and neurological mutant map. Twenty four ODDD linked Cx43 mutations have been evaluated as either producing or not producing CNS myelination issues. Black text labels indicate the various Cx43 mutations that are linked to CNS hypomyelination while the green labels indicate the Cx43 mutations that are CNS non-hypomyelination-linked. Mutations associated with neurological disorders appear to be randomly distributed throughout the Cx structure.

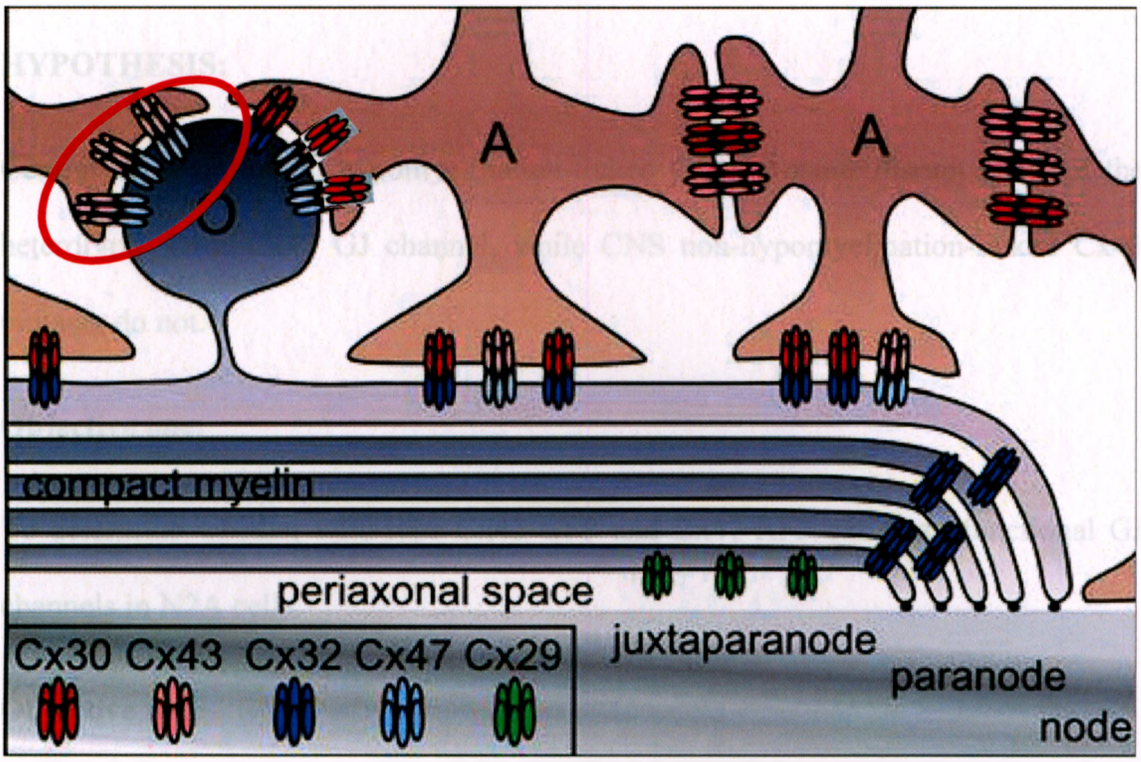

Modified from Orthmann-Murphy., et al 2008 and Scherer and Wasseft et al., 2011.

Figure 1-5: Connexin expression in macroglial cells. GJIC in astrocytes is mediated via Cx43/Cx43 or Cx30/30 homotypic GJ channels. Moreover, GJIC between A/O is mediated via both Cx32/Cx30 and Cx47/Cx43 heterotypic GJ channels and possibly Cx47/Cx30 GJ channels. Cx47/Cx43 GJs are thought to be the primary means of A/O GJIC. It has also been shown that reflexive GJs mediated by homotypic Cx32/Cx32 channels are present in oligodendrocytes. Oligodendrocyte Cx29 is not thought to contribute to the formation of GJ channels and may only form hemichannels at the cell surface.

1.12 Hypothesis and Objectives

HYPOTHESIS:

Central nervous system hypomyelination-linked Cx43 mutants disrupt GJIC of the heterotypic Cx43/Cx47 GJ channel, while CNS non-hypomyelination-linked Cx43 mutants do not.

Objective one:

- To determine whether wild-type Cx43-GFP and Cx47-RFP can form functional GJ channels in N2A cells.

Objective two:

- To determine whether CNS hypomyelination-linked Cx43-GFP mutants Cx43K134N-GFP, Cx43G138R-GFP or Cx43V96A-GFP can form functional homotypic GJ channels or heterotypic GJ channels with Cx47-RFP.

Objective three:

- To determine whether CNS non-hypomyelination-linked Cx43-GFP mutants Cx43R76H-GFP, Cx43V96M-GFP or Cx43H194P-GFP can form functional homotypic GJ channels or heterotypic GJ channels with Cx47-RFP.

2.0 Methods and Materials

2.1 Generation of cDNA Constructs: Cx47-GFP, Cx47-RFP

Human Cx47 cDNA was purchased from American Type Culture Collection (ATCC, Manassas, Virgina) and amplified using traditional polymerase chain reaction (PCR) with the following primers, forward, 5'-CTGGAATTCTTCTGGCCTGGAGAAGGAC-3' and reverse 5'-CCTGGTACCCAGCTCGCAAGCCAGCGCCCTCCGATCCACACGGTGGTC TTC-3', respectively. PCR cycles were run as follows; 94°C 30sec, 60°C 30sec, 72°C 90sec, for 25 cycles. In order to create the Cx47-GFP fusion protein the resulting cDNA was subcloned into the pEGFP-N1 vector using the EcoRI and KpnI restriction sites. The Cx47-GFP fusion protein with a 19 amino acid linker was confirmed by sequencing (NorClone Biotech Labs, London Ontario). The pTagRFP-N plasmid (Evrogen, Moscow, Russia) was used for the construction of the Cx47-RFP fusion protein. The human Cx47-RFP fusion protein was generated by isolation of Cx47 cDNA from the Cx47-GFP fusion construct mentioned above via double digestions of the EcoRI and KpnI restriction sites (Figure 2-1). Plasmid DNA was purified using QIAprep Spin Miniprep Kit (QIAGEN, Valencia, California) and subsequently subcloned into the EcoRI and KpnI restriction sites of the pTagRFP-N plasmid. The resulting Cx47-RFP construct was confirmed by sequencing.

2.2 Generation of cDNA Constructs: Cx43-GFP, Cx43K134N-GFP, Cx43V96A-GFP, Cx43V96M-GFP, Cx43G138R-GFP, Cx43R76H-GFP, Cx43H194-GFP

Connexin43 cDNA was amplified by traditional PCR with primers forward 5'-CGGGGTACCAACATGGGTGACTGGAGC-3 and reverse

5'-CGCGGATCCTTGATCTCCAGGTCATCA-3'. PCR cycles were run as follows, 94°C 30sec, 60°C 30sec, 72°C 90sec, for 25 cycles. The resultant cDNAs were subcloned into the pEGFP-N1 vector via the Kpn1 and BamH1 restriction sites (Clonetech, California, USA) in order to generate a GFP fusion protein with a 7 amino acid linker (Figure 2-2). The Cx43-GFP construct was confirmed by sequencing (Robarts Research, London Ontario). Six Cx43 mutants (table1), Cx43K134N-GFP, Cx43G138R-GFP, Cx43V96A-GFP, Cx43V96M-GFP, Cx43R76H-GFP, and Cx43H194P-GFP were generated using the using the QuikChange site-directed mutagenesis kit (Stratagene, La Jolla, California) (Figure 2-3). Mutant cDNAs were then amplified by traditional PCR, identical to the methods stated above. Resultant Cx43 cDNAs were inserted separately into the pEGFP-N1 vector (Clonetech, California, USA) via the Kpn1 and BamH1 restriction sites in order to generate a GFP fusion protein and then confirmed by sequencing (Norclone Biotech Labs, London Ontario / Robarts Research, London Ontario).

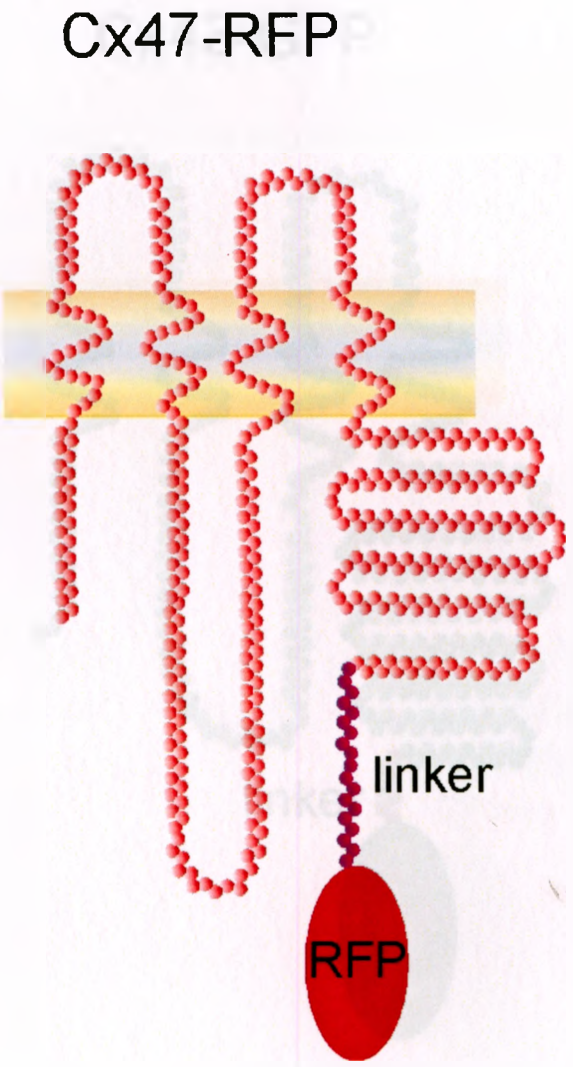

Figure 2-1: This figure represents a topological map of Cx47. In order to construct a RFP- fusion protein, Cx47 was inserted in the pTAG-RFP-N1 vector and subsequently fused to a RFP with a 19 amino acid linker.

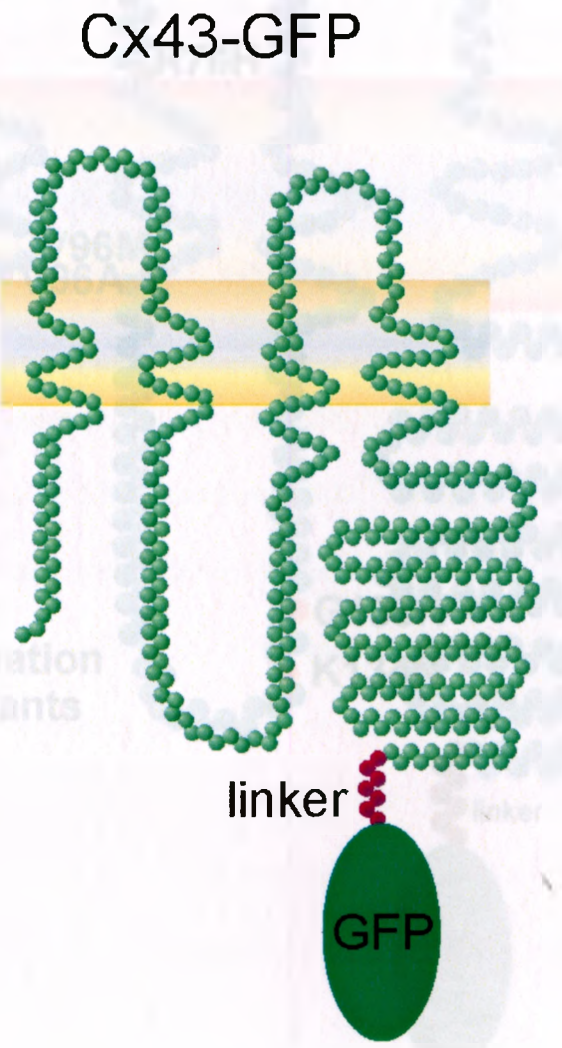

Figure 2-2: This figure represents a togological map of Cx43. In order to construct a GFP- fusion protein Cx43 was inserted in the pEGFP-N1 vector and subsequently fused to a GFP with a 7 amino acid linker.

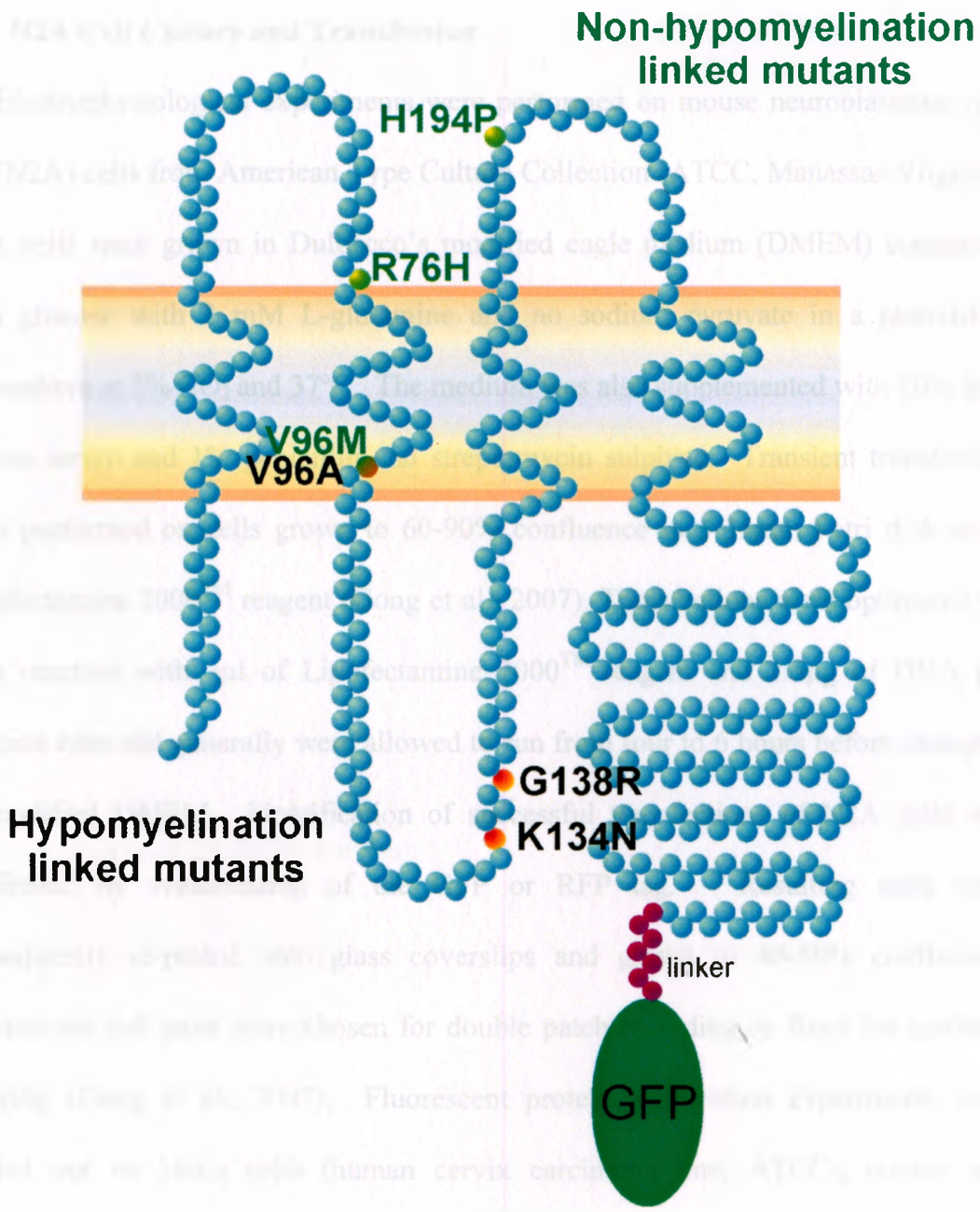

Figure 2-3: Cx43 topology and ODDD linked mutant map. Three CNS hypomyelination-linked Cx43 mutants (black text labels) have been chosen for imaging and functional studies (Cx43K134N, Cx43G138R, and Cx43V96A). In comparison to three CNS non-hypomyelination-linked Cx43 mutants (green text labels) include Cx43R76H, Cx43V96M, and Cx43H194P. All mutants were made in the pEGFP-N1 vector and had a GFP- tag with a 7 amino acid linker.

2.3 N2A Cell Culture and Transfection

Electrophysiological experiments were performed on mouse neuroblastoma type 2A (N2A) cells from American Type Culture Collection (ATCC, Manassas Virginia). N2A cells were grown in Dulbecco's modified eagle medium (DMEM) containing high glucose with 2 mM L-glutamine and no sodium pyruvate in a humidified atmosphere at 5% CO_2 and 37°C. The medium was also supplemented with 10% fetal bovine serum and 1% penicillin and streptomycin sulphate. Transient transfection were performed on cells grown to 60-90% confluence in a 35mm Petri dish using Lipofectamine 2000™ reagent (Gong et al., 2007). Transfections were optimized for each reaction with 3µl of Lipofectamine 2000™ reagent and 1.5µg of DNA per reaction tube and generally were allowed to run from four to 6 hours before changing to modified DMEM. Identification of successful transfections of N2A cells was confirmed by visualization of the GFP or RFP tag. Resulting cells were subsequently re-plated onto glass coverslips and grown to 40-50% confluence. Fluorescent cell pairs were chosen for double patch recording or fixed for confocal imaging (Gong et al., 2007). Fluorescent protein localization experiments were carried out on HeLa cells (human cervix carcinoma line, ATCC), culture and transfection conditions are identical to those used for the N2A cells.

2.4 Fixation and Fluorescent Imaging

After 24-36 hrs, transiently transfected cells were re-plated onto glass coverslips and allowed to reattach to the surface of the glass coverslip. After 12-24hrs, coverslips were transferred to a 24-well plate and cells were fixed with an 80% methanol / 20% acetone solution for 15 minutes at room temperature. The coverslips

were subsequently mounted onto glass slides using Vectashield with DAPI (Vector, Burlington, Ontario) and the outer edges were sealed using clear nail polish. Slides were then stored in a slidebox at 4°C for imaging. Cells were analyzed on a Zeiss LSM 510-meta confocal microscope (Zeiss, Thornwood, New York) mounted on an inverted Axiovert 200 motorized stage equipped with a 63x oil immersion (1.4 numerical aperture objective). Fluorescent signals were imaged by excitation at 488, 543, or 730 nm wavelengths, produced by argon, heliumneon, and Chameleon multiphoton lasers, respectively. The 488nm, 543nm, and 730nm laser lines are for detecting GFP, RFP, and DAPI, respectively. 543nm images were modified using ZEN software while phase contrast brightness was occasionally modified using CorelDraw X3™ software.

2.5 Electrophysiological Recording

Transiently transfected N2A cells were re-plated onto round glass coverslips (1 cm diameter) and grown to 40-50% confluence. After 2-24 hrs coverslips were transported to a 35mm Petri dish containing a bath solution consisting of, (mM) NaCl (135.0), KCl (5.0), HEPES (10.0), $MgCl_2$ (1.0), $CaCl_2$ (2.0), $BaCl_2$ (1.0), CsCl (2.0), Na pyruvate (2.0) and D-glucose (5.0). Petri dishes containing a submerged coverslip were transported to a dual whole-cell recording chamber and were visualized on a Leica DM IRB inverted microscope. Fluorescent cell pairs were chosen based upon a positive identification of fluorescent signals and a substantial cell-cell contact area (Figure 2-4). Those cells that were fluorescent but not closely apposing were not chosen for patch recordings (Figure 2-4). Heterotypic pairs were chosen if a red fluorescing and a green fluorescing cell were tightly apposed. Glass

pipettes with an outer diameter 1.5 mm and length 76 mm (World Precision Instruments, Sarasotta, Florida) were pulled into a patch electrode on a Narishige pp-83 pipette puller (Narishige, East Meadow, New York). Patch electrodes were filled with an internal solution composed of, (mM) , CsCl (130.0), HEPES (10.0), Mg-ATP (5.0), $CaCl_2$ (0.5), CsOH (10.0) and typically were pulled to a resistance of 2-5 MΩ. For conductance measurements dual whole cell-recordings were obtained using two Axopatch 200B amplifiers and pClamp 9.0 software (Molecular Devices, Sunnyvale, California). Both of the paired cells were initially voltage-clamped at 0 mV while one cell underwent a series of voltage steps between -100 mV and + 100 mV with 20 mV increments for 5 to 10s to establish a transjunctional voltage (V_j). The transjunctional current (I_j) was recorded from the second cell (Figure 2-5). Intervals between steps ranged from 15 to 30s. Macroscopic transjunctional conductance (G_j) was calculated by dividing the measured junctional current by the transjunctional voltage (V_j): $G_j = I_j / V_j$. The G_j for each cell pair was recorded and the mean for each GJ channel type was calculated.

2.6 Statistics

Group statistics were expressed as mean ± S.E.M. All statistical data were obtained using GraphPad Prism 4.0 (San Diego, CA). One-way analysis of variance (ANOVA) tests were used to compare groups for statistical differences (p-values stated), and Tukey's post-hoc test was performed in order to compare the differences among multiple groups. Differences between groups are denoted by the uppercase alphabetical characters, A, B, and C.

Cx43 Mutant	Forward (5'- 3')	Reverse (5'-3')
Cx43K134N-GFP	TGAGATAAAGAATT TCAAGTACGGT	ACCGTACTTGAAATT CTTTATCTCA
Cx43G138R-GFP	GAAGTTCAAGTACA GGATTGAAGAGCAT G	CCATGCTCTTCAATC CTGTACTTGAACTT
Cx43V96A-GFP	CACTCTTGTACCTG GCTCATGCCTTCTAT GTGATGCGAAAGGA AG	CTTCCTTTCGCATCA CATAGAAGGCATGA GCCAGGTACAAGAG TG
Cx43V96M-GFP	CACACTCTTGTACCT GGCTCATATGTTCT ATGTGATGCGAAAG G	CCTTTCGCATCACAT AGAACATATGAGCC AGGTACAAGAGTGT G
Cx43R76H-GFP	TTCCCAATCTCTCAT GTGCACTTCTGGGT CCTGCAGATC	GATCTGCAGGACCCA GAAGTGCACATGAG AGATTGGGAA
Cx43H194P-GFP	CAAAAGAGATCCCT GCCCACCTCAGGTG GACTGTTTCCTC	GAGGAAACAGTCCA CCTGAGGTGGGCAG GGATCTCTTTTG

Table 2-1: *Primers used to generate Cx43 mutants.* The forward and reverse primers for the generation of the following Cx43 mutants, Cx43K134N-GFP, Cx43G138R-GFP, Cx43V96A-GFP, Cx43V96M-GFP, Cx43R76H-GFP, and Cx43H194P-GFP are listed. All mutant cDNA was subcloned into the pEGFP-N1 vector using Kpn1 and BamH1 restrictions sites.

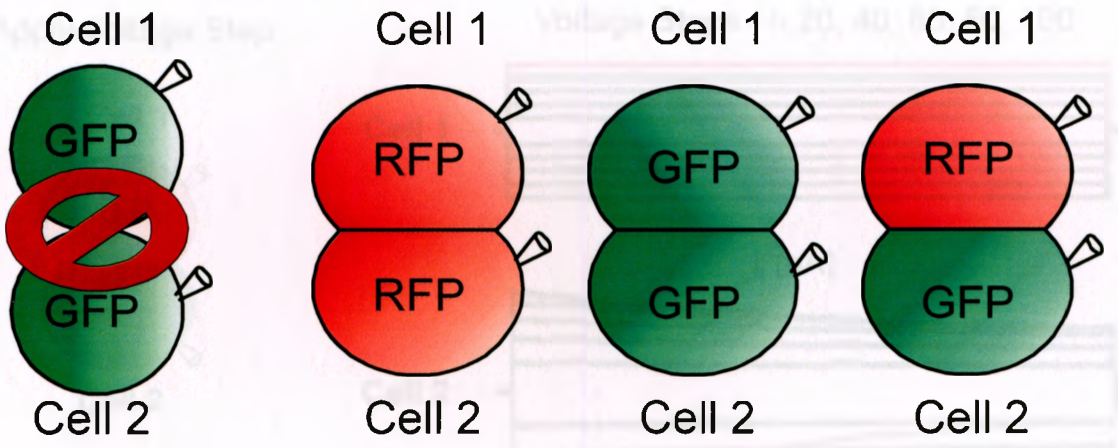

Figure 2-4: Cell pair selection for electrophysiological recordings. Non-desirable cell pairs are recognized as fluorescent yet do not have tightly apposed cell-cell membranes, indicated by the first cell pair in the sequence. For both homomeric homotypic and homomeric heterotypic GJ configurations only fluorescent cell pairs with closely apposed cell-cell membranes were chosen for electrophysiological recording. This selection greatly raises the percentage of GJ coupling between fluorescent positive cell pairs. Cx47 constructs all contain an RFP tag where as Cx43 constructs all contain a GFP tag.

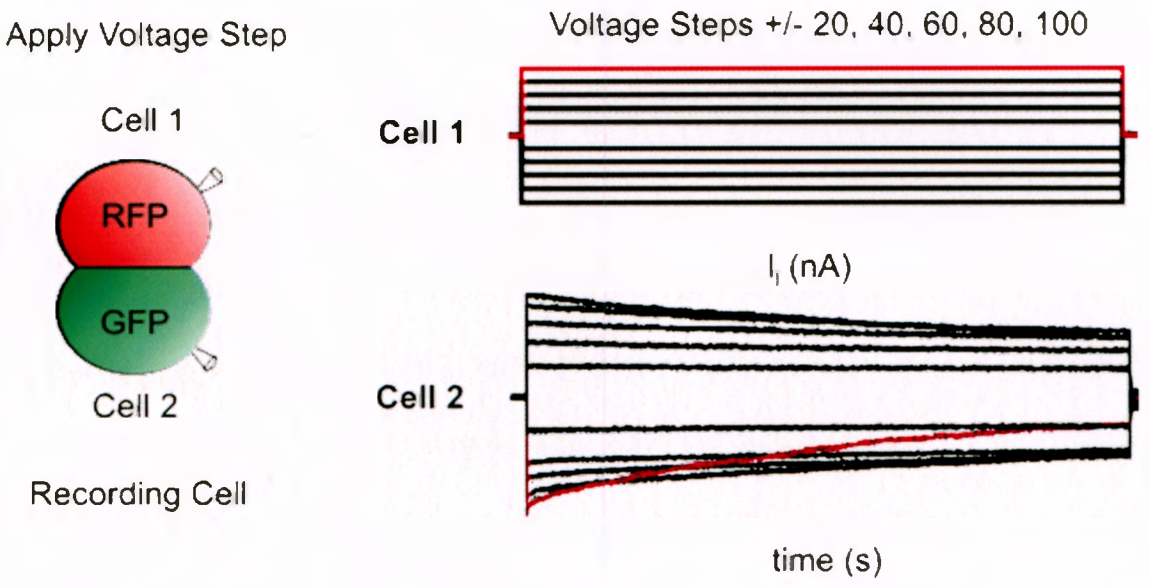

Figure 2-5: Dual whole-cell patch clamp recordings. Homotypic cell pairs (same colour) or heterotypic cell pairs (two colours) were chosen for electrophysiological recording. Initially, cell 1 and cell 2 are voltage clamped at 0 mV in order to prevent any transjunctional current. After obtaining a Giga-Ohm seal the whole cell configuration was obtained by the application of negative pressure. Voltage steps are applied to cell 1 and transjunctional current is measured and recorded from cell 2. Red lines outline the application of +100 mV voltage step to cell 1 and the response recorded from cell 2.

3.0 Results

3.1 Cx43-GFP and Cx47-RFP Form Homotypic or Heterotypic Cx43-GFP/Cx47-RFP GJ Plaque-like Structures in HeLa and N2A cells.

To facilitate the identification of Cx43 and or Cx47 expressing cells, we engineered green fluorescent protein (GFP) and red fluorescent protein (RFP) genes at the carboxyl terminals of Cx43 and Cx47 genes to form Cx43-GFP and Cx47-RFP, respectively. Red fluorescent signals were observed in intracellular compartments, cell surface and cell-cell junctions in HeLa cells transiently expressing the Cx47-RFP fusion protein. Indicating that Cx47-RFP was able to traffic to cell surface and form homotypic Cx47-RFP gap junction plaques (Figure 3-1A). GJ plaque-like structures are readily identifiable at the cell-cell interface.

HeLa cells transiently expressing Cx43-GFP form homotypic Cx43-GFP GJ plaque like structures at the cell-cell interface (Figure 3-1A). When HeLa cells transiently expressing Cx43-GFP were plated with the HeLa cells transiently expressing Cx47-RFP, GJ plaque-like structures with both red and green fluorescent signals were observed between Cx43-GFP and Cx47-RFP expressing cell pairs (Figure 3-1B), indicating that Cx43-GFP is likely to be able to form heterotypic GJ channels with Cx47-RFP. The formation of heterotypic plaque like structures was not as frequently as the homotypic GJ channel configurations.

Figure 3-1: Communication deficient HeLa cells were transiently transfected with *hCx47-RFP or hCx43-GFP.* Cellular localization of each Cx construct was then determined by epifluoresence. **(A)** The arrow indicates the presence of GJ plaques at the cell-cell interface. GJ plaque-like structures are present in HeLa cells forming the homotypic GJ channels, Cx43-GFP/Cx43-GFP and Cx47-RFP/Cx47-RFP. **(B)** Apparent heterotypic GJ plaques are present between HeLa cells expressing Cx43-GFP and Cx47-RFP, respectively. Corresponding phase contrast images (greyscale images) for each fluorescent image are included and illustrate cell morphology, scale bars = 10 μm.

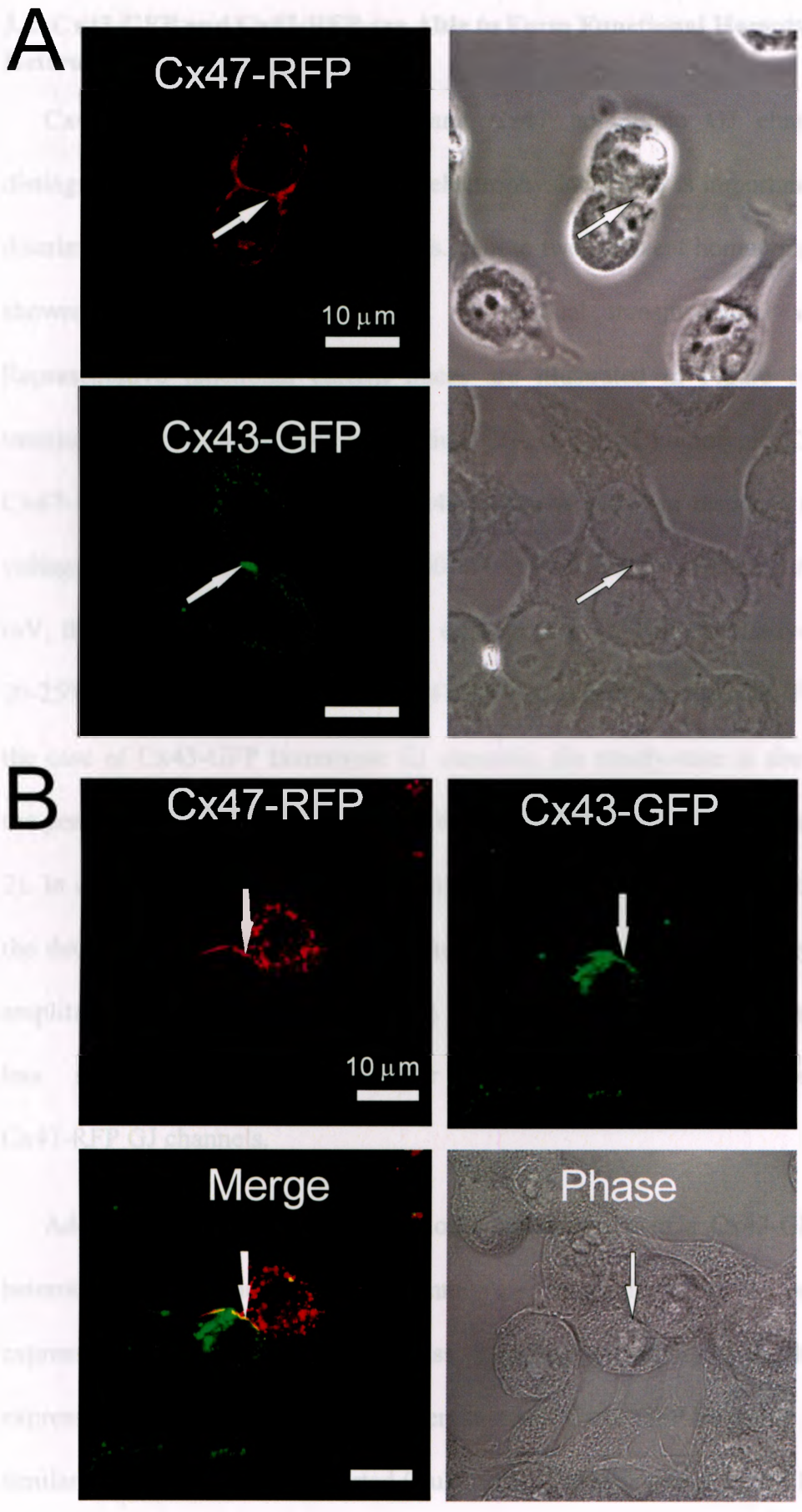
A
Cx47-RFP
10 μm
Cx43-GFP
B
Cx47-RFP
10 μm
Cx43-GFP
Merge
Phase

3.2 Cx43-GFP and Cx47-RFP are Able to Form Functional Homotypic and Heterotypic GJ channels.

Cx43 homotypic GJ channels and Cx47 homotypic GJ channels can be distinguished via double-patch clamp electrophysiology. It is important to be able to discriminate between GJ channel types. These two different homotypic GJ channels showed different gating sensitivity to identical transjunctional voltage steps. Representative junctional current traces are illustrated in Figure 3-2A to show transjunctional voltage-dependent gating (V_j-gating) of homotypic Cx43-GFP and Cx47-RFP as well as heterotypic Cx43-GFP/Cx47-RFP in response to a series of voltage steps (V_j) from 0 to ± 20 - 100 mV (with 20 mV increment). At a V_j of 100 mV, the junctional current amplitude decreased to an average steady-state level of 20-25% of the peak amplitude for Cx47-RFP homotypic GJ channel (Figure 3-2). In the case of Cx43-GFP homotypic GJ channels, the steady-state is about 40-50% of the peak amplitude and it took about twice as long to reach a steady-state (Figure 3-2). In order to high-light the differences in the steady-state level and the kinetics of the decay process, initial junctional current responses were normalized to the peak amplitude and superimposed in Figure 3-2. Clearly, Cx43-GFP GJ channels showed less sensitivity to V_j and a slower kinetics of V_j-gating compared to that of Cx47-RFP GJ channels.

Additionally, representative junctional current trace of a Cx43-GFP/Cx47-RFP heterotypic GJ channel show an asymmetrical sensitivity to V_j. As predicted, cells expressing Cx43-GFP side show less V_j-gating sensitivity than the Cx47-RFP expressing cells (Figure 3-2). Our observations of Cx43-GFP V_j-gating properties are similar to those previously reported (Bukauskas, Bukauskiene et al. 2001; Gong, Shao

et al. 2007). Preliminary data also illustrates that Cx47-RFP behaves similarly to untagged Cx47, indicating that the fluorescent tag does not have a large effect on the junctional current sensitivity to absolute V_j pulses.

Figure 3-2: Representative junctional current traces in response to a voltage step protocol (the V_j), with an initial holding potential of 0 mV and increasing in increments of 20 mV from ± 20 mV to ±100 mV. (**A**) A set of representative junctional current traces of Cx47-RFP homotypic GJ channels is shown. When the absolute value of V_j was higher than 60 mV, the junctional current decreases with time and reaches a much lower level steady state. (**B**) A set of representative junctional current traces of a Cx43-GFP homotypic GJ channel is shown. The junctional currents take a lot longer to reach an apparent steady state. (**C**) A set of representative current traces of a heterotypic Cx43-GFP/Cx47-RFP heterotypic GJ channel is illustrated. Asymmetrical voltage dependent gating is observed where Cx43-GFP is less sensitive to the V_j and Cx47-RFP maintains higher sensitivity to V_j. (**D**) Superimposed macroscopic junctional current traces normalized to the peak current amplitude is shown for Cx43-GFP (green trace) and Cx47-RFP (red trace) homotypic GJ channels in response to a -100 mV voltage step. A much lower steady state level and a more rapid decay were observed for Cx47-RFP homotypic GJ channels in comparison to Cx43-GFP.

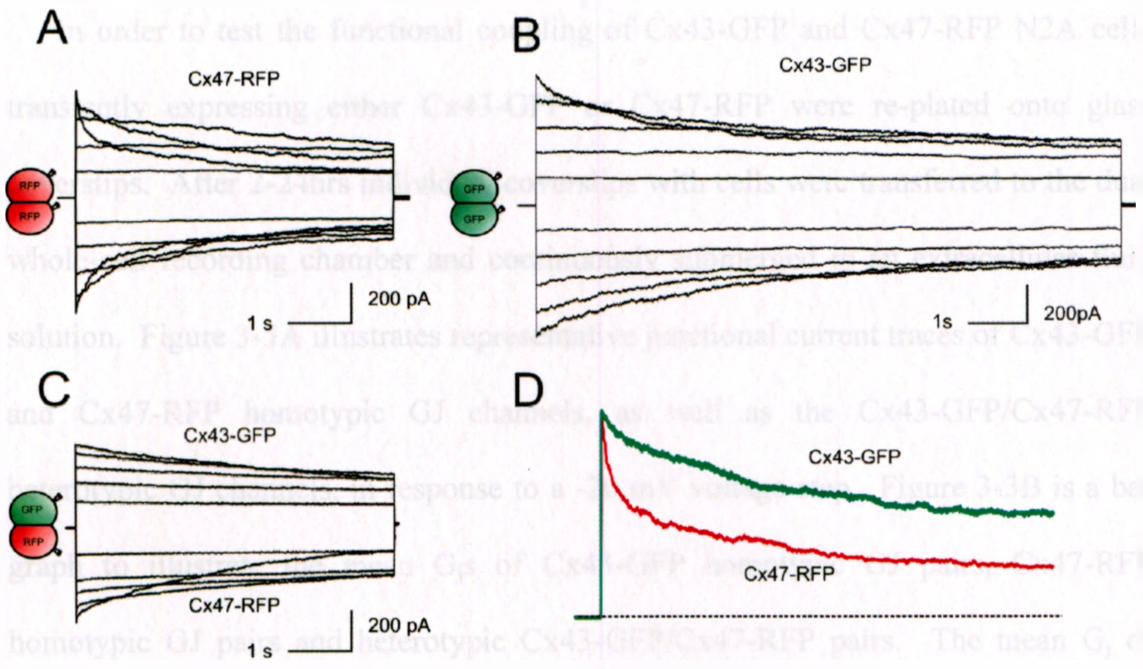
A
Cx47-RFP
RFP
RFP
200 pA
1 s
B
Cx43-GFP
GFP
GFP
1s
200pA
C
Cx43-GFP
GFP
RFP
Cx47-RFP
200 pA
1 s
D
Cx43-GFP
Cx47-RFP

In order to test the functional coupling of Cx43-GFP and Cx47-RFP N2A cells transiently expressing either Cx43-GFP or Cx47-RFP were re-plated onto glass coverslips. After 2-24hrs individual coverslips with cells were transferred to the dual whole-cell recording chamber and continuously submerged in an extracellular fluid solution. Figure 3-3A illustrates representative junctional current traces of Cx43-GFP and Cx47-RFP homotypic GJ channels, as well as the Cx43-GFP/Cx47-RFP heterotypic GJ channels, in response to a -20 mV voltage step. Figure 3-3B is a bar graph to illustrate the mean G_js of Cx43-GFP homotypic GJ pairs, Cx47-RFP homotypic GJ pairs and heterotypic Cx43-GFP/Cx47-RFP pairs. The mean G_j of Cx43-GFP homotypic cell pairs was found to be 18.8 ± 0.8 nS (n = 50 from 11 independent transfections). The mean G_j of homotypic Cx47-RFP cell pairs, 6.4 ± 1.3 nS (n=20 from 6 independent transfections) and the mean G_j of Cx43-GFP/Cx47-RFP cell pairs was shown to be 5.1 ± 0.6 nS (n=21 from 6 independent transfections). Significant differences were found between each of the following, Cx43-GFP vs. Cx47-RFP ($p<0.001$), Cx43-GFP vs. Cx43-GFP/Cx47-RFP ($p<0.001$) with one-way ANOVA followed by Tukeys post-hoc test. The difference between groups is distinguished in figure 3-3 by an A vs. B labelling system. No significant difference was found between the Gj of Cx47-RFP homotypic channels and the Gj of Cx43-GFP/Cx47-RFP heterotypic channels ($p=0.054$). It is clear that Cx43-GFP and Cx47-RFP are able to form functional homotypic GJ channels and heterotypic Cx43-GFP/Cx47-RFP GJ channels in our N2A model cell system.

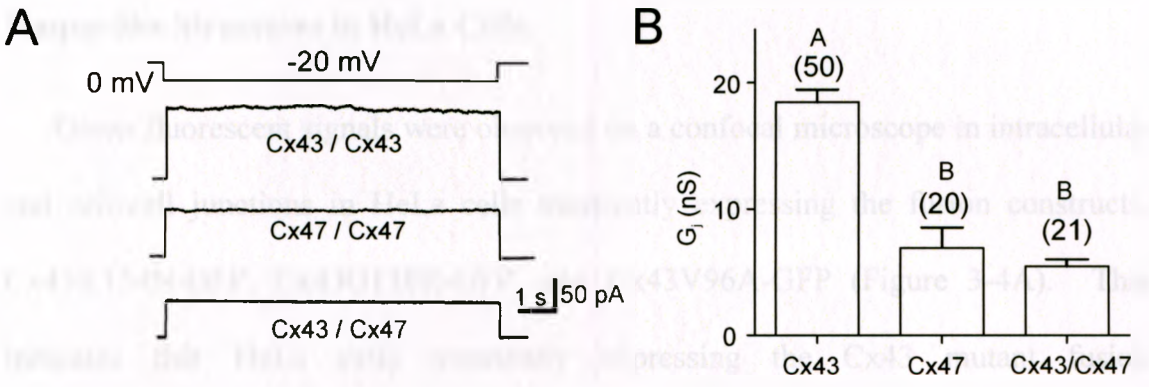

Figure 3-3: Junctional conductance (G_j) measurements between wild-type Cx43-GFP and Cx47-RFP in both the homotypic and heterotypic GJ channel configurations. **(A)** Cx43-GFP and Cx47-RFP do form functional heterotypic GJ channels in N2A cells. Representative macroscopic junctional current traces of two homotypic GJ channels, Cx43-GFP/Cx43-GFP , Cx47-RFP/Cx47-RFP as wells as the heterotypic Cx43-GFP/Cx47-RFP GJ channel in response to a -20 mV voltage step. **(B)** The mean G_j in response to a -20 mV voltage step of homotypic Cx43 = 18.8 ± 0.8 nS (n=50), Cx47= 6.4 ± 1.3 (n=20) GJ channels is shown and the average G_j of the Cx43/Cx47 heterotypic GJ channel= 5.1 ± 0.6 nS (n=21). A one-way ANOVA with a Tukeys post-hoc test confirms that Cx43-GFP/Cx43-GFP vs. Cx47-RFP/Cx47-RFP ($p < 0.001$), Cx43-GFP/Cx43-GFP vs. Cx43-GFP/Cx47-RFP ($p < 0.001$) are significantly different where differences are designated by A vs. B. However, Cx47-RFP/Cx47-RFP vs. Cx43-GFP/Cx47-RFP was not found to be significantly different.

3.3 Hypomyelination-linked Cx43 Mutants Appear to Form Homotypic GJ Plaque-like Structures in HeLa Cells.

Green fluorescent signals were observed on a confocal microscope in intracellular and cell-cell junctions in HeLa cells transiently expressing the fusion constructs, Cx43K134N-GFP, Cx43G138R-GFP, and Cx43V96A-GFP (Figure 3-4A). This indicates that HeLa cells transiently expressing the Cx43 mutant fusion hypomyelination-linked constructs are able to traffic to the cell-cell surface and form homotypic GJ plaques. Figure 3-4 also illustrates a dim distribution of Cx43-GFP K134N and Cx43V96A-GFP at the cell periphery. HeLa cells transiently expressing the Cx43G138R-GFP fusion construct formed homotypic GJ plaque-like structures. However, the Cx43G138R-GFP mutant demonstrated a greater overall distribution at the cell membrane and the presence of actual GJ plaques is inconclusive.

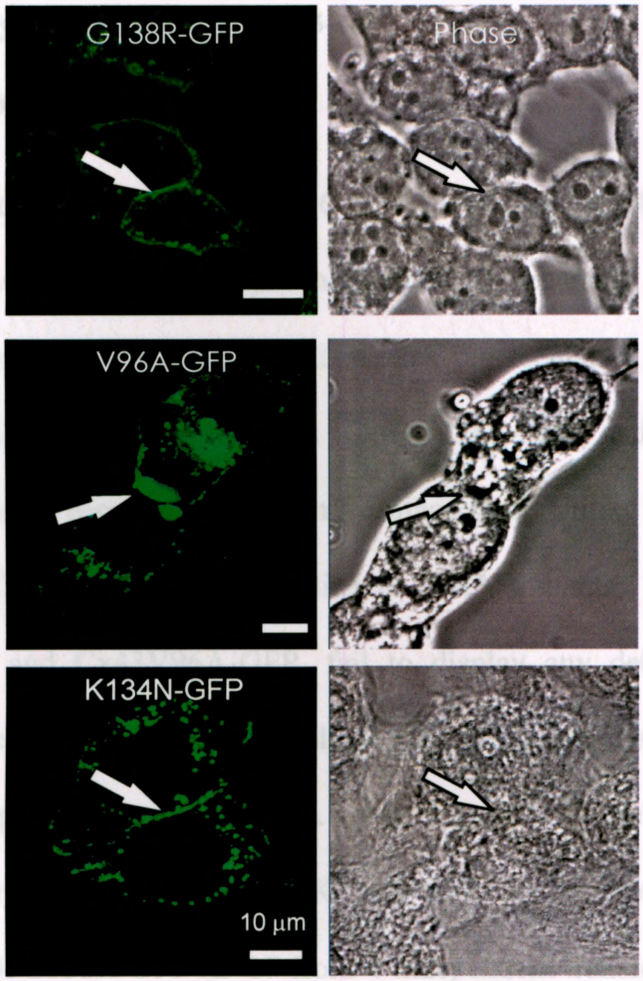

Figure 3-4: Confocal imaging of CNS hypomyelination-linked Cx43 mutants in the homotypic GJ channel configuration. Cellular localization of HeLa cells expressing the fusion constructs Cx43K134N-GFP, Cx43G138R-GFP, or Cx43V96A-GFP are visualized via confocal microscopy. The arrow indicates the presence of GJ plaque like structures at the cell-cell interface. It does appear the Cx43K134N-GFP and Cx43V96A-GFP form GJ plaques in HeLa cells. However, it is inconclusive whether Cx43G138R-GFP is able form GJ plaques as it demonstrates a uniform distribution at the cell border. The arrow indicates the presence of GJ plaque-like structures, all scale bars=10µm. Corresponding phase contrast images (greyscale images on the right panels) for each fluorescent image are included illustrate cell morphology.

3.4 CNS Hypomyelination-linked Cx43-GFP Mutants do not Form Functional Homotypic GJ Channels.

N2A cells expressing Cx43-GFP, Cx43K134N-GFP, Cx43G138R-GFP, or Cx43V96A-GFP were used to analyze homotypic GJ channel configurations via double-patch recordings. Figure 3-5A, illustrates representative junctional current traces of Cx43-GFP, Cx43K134N-GFP, Cx43G138R-GFP and Cx43V96A-GFP homotypic cell pairs in response to a -20 mV voltage step. Unlike wildtype Cx43, all of the selected CNS hypomyelination-linked Cx43 mutants, Cx43K134N-GFP, Cx43G138R-GFP and Cx43V96A-GFP, fail to display any detectable junctional current in response to a transjunctional voltage step, indicating that they do not form functional homotypic GJ channels in N2A cells. Figure 3-5B shows the mean G_j of Cx43-GFP homotypic GJ pairs, Cx43K134N-GFP (n=26 from 6 independent transfections), Cx43G138R-GFP (n=17 from 4 independent transfections) and lastly, Cx43V96A-GFP (n=23 from 5 independent transfections). The mean G_j of Cx43-GFP homotypic GJ channels were found to be 18.8 ± 0.8 nS. While the mean G_j of the three homotypic GJ channels composed of CNS hypomyelination-linked Cx43 mutants Cx43K134N-GFP, Cx43G138R-GFP, and Cx43V96A-GFP were found to be completely uncoupled. A one-way ANOVA with a Tukeys post-hoc test was performed to compare differences among groups. Significant differences were found between each of the following; Cx43-GFP vs. Cx43-GFP K134N ($p<0.001$), Cx43-GFP vs. Cx43-GFP G138R ($p<0.001$) and Cx43-GFP vs. Cx43-GFP V96A which are distinguished by an A vs. B designation. It is evident that the Cx43-GFP mutants K134N, G138R, and V96A are unable to form functional GJ channels in N2A cells.

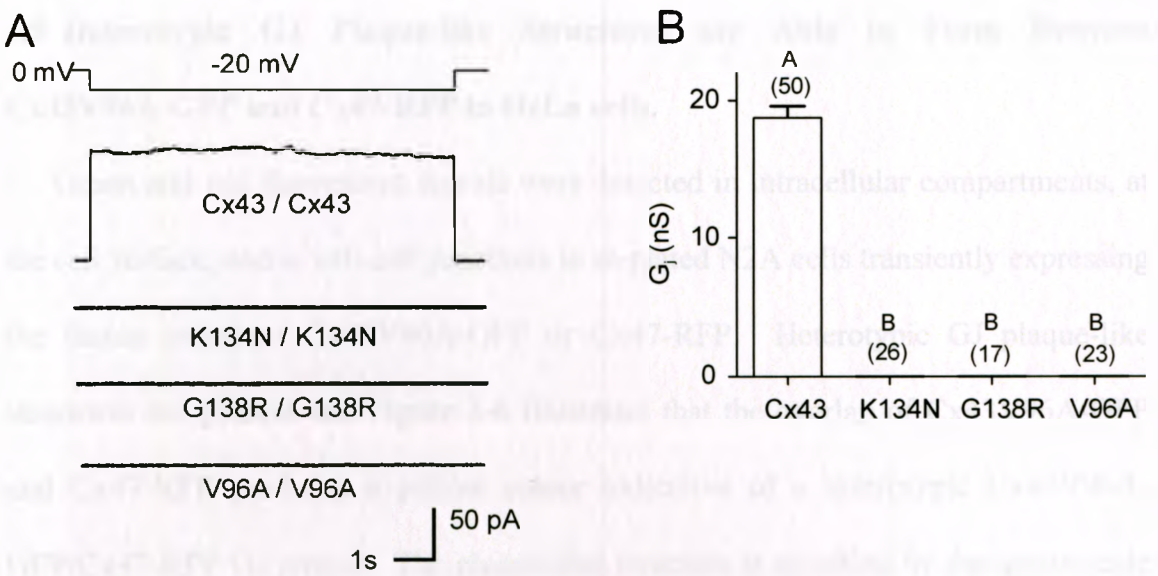

Figure 3-5: Junctional conductance (G_j) measurements between hypomyelination-linked Cx43 mutants in the homotypic GJ channel configuration **(A)** Cx43K134N-GFP, Cx43G138R-GFP, and Cx43V96A-GFP do not form functional homotypic GJ channels. Representative macroscopic junctional current traces of four homotypic GJ channels illustrate Cx43-GFP/Cx43-GFP, Cx43K134N-GFP/Cx43K134N-GFP, Cx43G138R-GFP/Cx43G138R-GFP and Cx43V96A-GFP/Cx43V96A-GFP in response to a -20 mV voltage step. **(B)** The mean G_j of homotypic Cx43-GFP/Cx43-GFP = 18.8 ± 0.8 nS (n=50), Cx43K134N-GFP / Cx43K134N-GFP = 0 nS (n= 26), Cx43G138R-GFP/ Cx43G138R-GFP = 0 nS (n=17 cell pairs) and Cx43V96A-GFP / Cx43V96A-GFP = 0 nS (n=23). A one-way ANOVA with a Tukeys post-hoc test confirmed that there was a significant difference between, Cx43-GFP vs.Cx43K134N-GFP ($p<0.001$) and Cx43-GFP vs. Cx43G138R-GFP ($p<0.001$) where differences are designated by A vs. B.

3.5 Heterotypic GJ Plaque-like Structures are Able to Form Between Cx43V96A-GFP and Cx47-RFP in HeLa cells.

Green and red fluorescent signals were detected in intracellular compartments, at the cell surface, and at cell-cell junctions in re-plated N2A cells transiently expressing the fusion construct Cx43V96A-GFP or Cx47-RFP. Heterotypic GJ plaque-like structures are present and Figure 3-6 illustrates that the overlap of Cx43V96A-GFP and Cx47-RFP produces a yellow colour indicative of a heterotypic Cx43V96A-GFP/Cx47-RFP GJ plaque. The plaque-like structure is specified by the arrow scale bars=10μm. There is also yellow vesicular like structures in both cells which indicate endocytosis of Cx43V96A-GFP/Cx47-RFP channels.

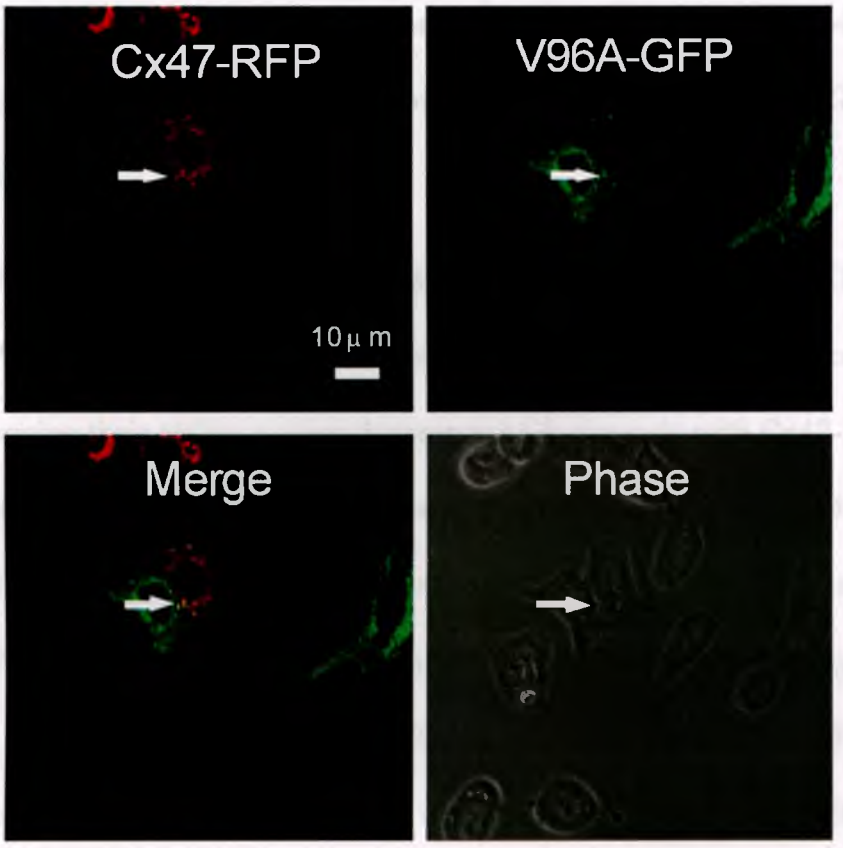

Figure 3-6: Confocal imaging of hypomyelination-linked Cx43 mutants in the heterotypic GJ channel configuration with Cx47-RFP. Cx43V96A-GFP appears to form heterotypic GJ plaques (yellow) with Cx47-RFP in HeLa cells. Vesicular structures likely containing endocytosed heterotypic GJ plaques were also present. The arrow indicates the presence of a heterotypic GJ plaque-like structure, all scale bars=10µm.

3.6 Dual Whole-cell Patch Clamp Reveals that CNS non-hypomyelination-linked Cx43 Mutants do not Form Functional Heterotypic GJ Channels with Cx47-RFP.

N2A cells transiently expressing Cx43-GFP, Cx43K134N-GFP, Cx43G138R-GFP, or Cx43V96A-GFP were analyzed via dual whole-cell recording in order to determine their ability to form heterotypic GJ channels with Cx47-RFP. Figure 3-7A illustrates representative junctional current traces of Cx43-GFP/Cx47-RFP, Cx43K134N-GFP/Cx47-RFP, Cx43G138R-GFP/Cx47-RFP, and Cx43V96A-GFP/Cx47-RFP heterotypic cell pairs in response to a -20 mV voltage step. It is clear that Cx43K134N-GFP, Cx43G138R-GFP, and Cx43V96A-GFP did not form functional heterotypic channels with Cx47-RFP in N2A cells. Figure 3-7B demonstrates the mean G_j of Cx43-GFP/Cx47-RFP (n=21 from 6 independent transfections), Cx43K134N-GFP/Cx47-RFP (n=13 from 4 independent transfections), Cx43G138R-GFP/Cx47-RFP (n=11 from 3 independent transfections), and Cx43V96A-GFP/Cx47-RFP (n=10 from 3 independent transfections) heterotypic GJ pairs. The mean G_j of Cx43-GFP/Cx47-RFP heterotypic GJ channels was found to be 5.5 ± 0.6 nS. The mean G_j of the heterotypic GJ channels formed between Cx47-RFP and any one of the Cx43K134N-GFP, Cx43G138R-GFP, and Cx43V96A-GFP mutants hypomyelination-linked mutants was found to be 0 nS. A one-way ANOVA was performed to compare with a Tukeys post-hoc test. Significant differences were found between each of the following; Cx43-GFP/Cx47-RFP vs. Cx43K134N-GFP/Cx47-RFP ($p<0.001$), Cx43-GFP/Cx47-RFP vs. Cx43G138R-GFP/Cx47-RFP

($p<0.001$), and Cx43-GFP/Cx47-RFP vs. Cx43V96A-GFP/Cx47-RFP ($p<0.001$) where differences are designated by A vs. B vs. C.

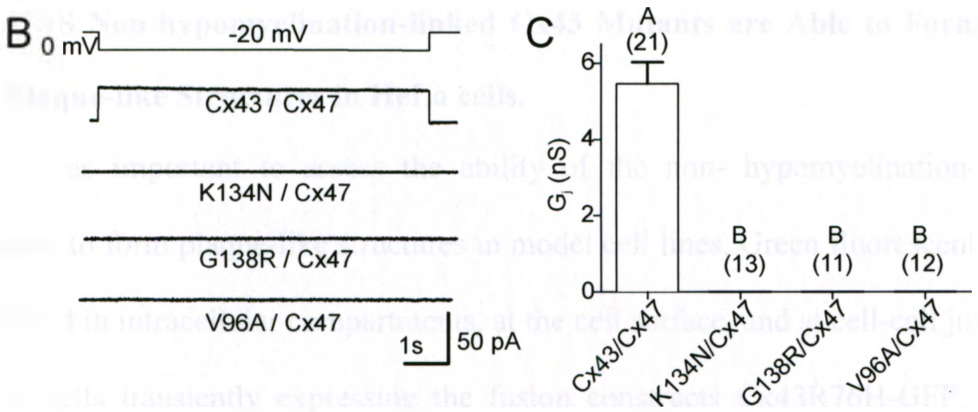

Figure 3-7: Junctional conductance (G_j) traces between hypomyelination-linked Cx43 mutants in the heterotypic GJ channel configuration with Cx47-RFP **(A)** N2A cells expressing the fusion constructs Cx43K134N-GFP, Cx43G138R-GFP or Cx43V96A-GFP do not form functional heterotypic GJ channels with Cx47-RFP. Representative junctional current traces in response to a -20 mV voltage step (V_j) of four heterotypic GJ channels. Where Cx43-GFP/Cx47-RFP shows a small mean conductance yet junctional traces representing, Cx43K134N-GFP/Cx47-RFP, Cx43G138R-GFP/Cx47-RFP, or Cx43V96A-GFP/Cx47-RFP illustrate that heterotypic GJ channels formed between Cx47-RFP and CNS hypomyelination-linked Cx43 mutants do not form functional GJ channels in N2A cells. **(B)** The average G_j of four heterotypic GJ channels is displayed as a mean where, Cx43-GFP/Cx47-RFP = 5.1 ± 0.6 nS (n=21), Cx43K134N-GFP/Cx47-RFP = 0 nS (n=13), Cx43G138R-GFP/Cx47-RFP = 0 nS (n=11), and Cx43V96A-GFP/Cx47-RFP = 0 nS (n=12). A one-way ANOVA with a Tukeys post-hoc test confirmed that there was a significant difference between, Cx43-GFP/Cx47-RFP vs.Cx43K134N-GFP /Cx47-RFP ($p<0.001$) and between Cx43-GFP/Cx47-RFP vs. Cx43G138R-GFP/Cx47-RFP ($p<0.001$) and Cx43-GFP/Cx47-RFP vs. Cx43V96A-GFP/Cx47-RFP ($p<0.001$) and differences are designated by A vs. B vs. C.

3.7 CNS Non-hypomyelination-linked Cx43 Mutants are Able to Form Homotypic GJ Plaque-like Structures in HeLa cells.

It was important to assess the ability of the non- hypomyelination-linked Cx43 mutants to form plaque-like structures in model cell lines. Green fluorescent signals were observed in intracellular compartments, at the cell surface, and at cell-cell junctions in the HeLa cells transiently expressing the fusion constructs Cx43R76H-GFP, Cx43V96M-GFP, or Cx43H194P-GFP. Figure 3-8 contains representative confocal images of HeLa cell pairs transiently expressing Cx43R76H-GFP, Cx43V96M-GFP, or Cx43H194P-GFP. Interestingly, HeLa cells expressing the Cx43H194P-GFP fusion construct appear to show a greater intracellular distribution compared to Cx43-GFP. Overall, confocal microscopy study indicates that all three selected Cx43 mutants that are not linked to CNS hypomyelination do appear to be able to form homotypic GJ channels in the HeLa cells. The arrow indicates the presence of plaque-like structures at the cell-cell interfaces (Figure 3-8).

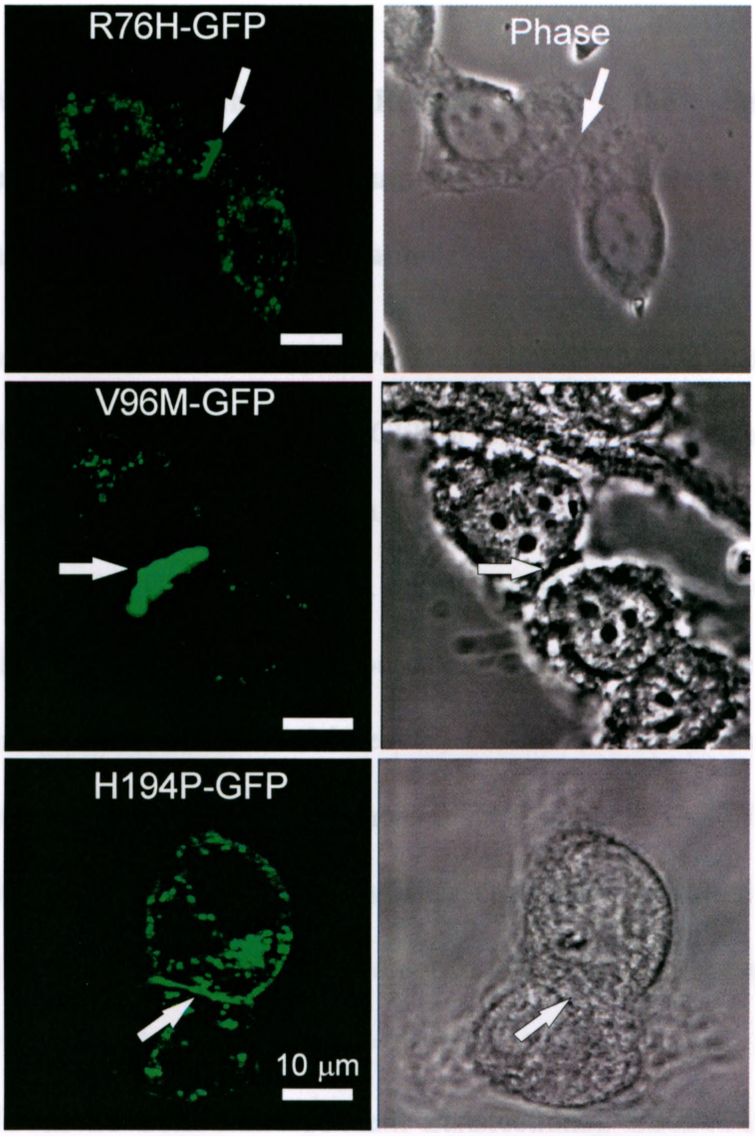

Figure 3-8: Confocal imaging of non-hypomyelination-linked Cx43 mutants in the homotypic GJ channel configuration. Cellular localization of HeLa cells expressing the fusion construct Cx43R76H-GFP, Cx43V96M-GFP or Cx43H194P-GFP. The arrow indicates the presence of GJ plaque-like structures at the cell-cell interface. It does appear Cx43R76H-GFP, Cx43V96M-GFP, or Cx43H194P-GFP is able to form GJ plaques in HeLa cells. The arrow indicates the presence of GJ plaque-like structures and all scale bars=10µm. Corresponding phase contrast images (greyscale images) for each fluorescent image are included and illustrate cell morphology

3.8 Dual Whole-cell Technique Reveals that the Selected CNS Non-hypomyelination-linked Cx43 Mutants Show Completely or Partially Impaired Functional Homotypic GJ Channels

To test the ability of the non-hypomyelination-linked Cx43 mutants, N2A cells expressing Cx43R76H-GFP, Cx43V96M-GFP or Cx43H194P-GFP were analyzed in the homotypic GJ channel configuration. Figure 3-9A, illustrates representative traces of Cx43-GFP, Cx43R76H-GFP, Cx43V96M-GFP or Cx43H194P-GFP homotypic cell pairs channels in response to a -20 mV voltage step, to test functionality of the GJ channel. Moreover, Cx43R76H-GFP was able to form functional homotypic GJ channels while the two Cx43 mutants, Cx43V96M-GFP and Cx43H194P-GFP homotypic GJ channels were completely impaired in N2A cells expressing the non-hypomyelination-linked constructs. Fig 3-9B shows the mean G_j of Cx43-GFP homotypic GJ pairs (n=50 from 11 independent transfections), Cx43R76H-GFP (n=21 from 5 independent transfections), Cx43V96M-GFP (n=16 from 4 independent transfections) and lastly, Cx43H194P-GFP (n=13 from 3 independent transfections). The mean G_j of Cx43-GFP homotypic GJ channels is 18.8 ± 0.8 nS, while the mean G_j of the Cx43-GFP R76H homotypic GJ channels was found to be 1.7 ± 0.2 nS. Conversely, Cx43V96M-GFP and Cx43H194P-GFP were found to have a mean homotypic GJ conductance of 0 nS. A one-way ANOVA was performed with a Tukeys post-hoc test to compare differences among groups. Significant differences were found between each of the following, Cx43-GFP vs. Cx43R76H-GFP ($p<0.001$), Cx43-GFP vs. Cx43V96M-GFP ($p<0.001$) and Cx43-

GFP vs. Cx43H194P-GFP ($p<0.001$). It appears that only one of the selected specific CNS hypomyelination-linked Cx43 mutants was able to form functional homotypic channels. However, the conductance level is much reduced compare to that of wild-type Cx43.

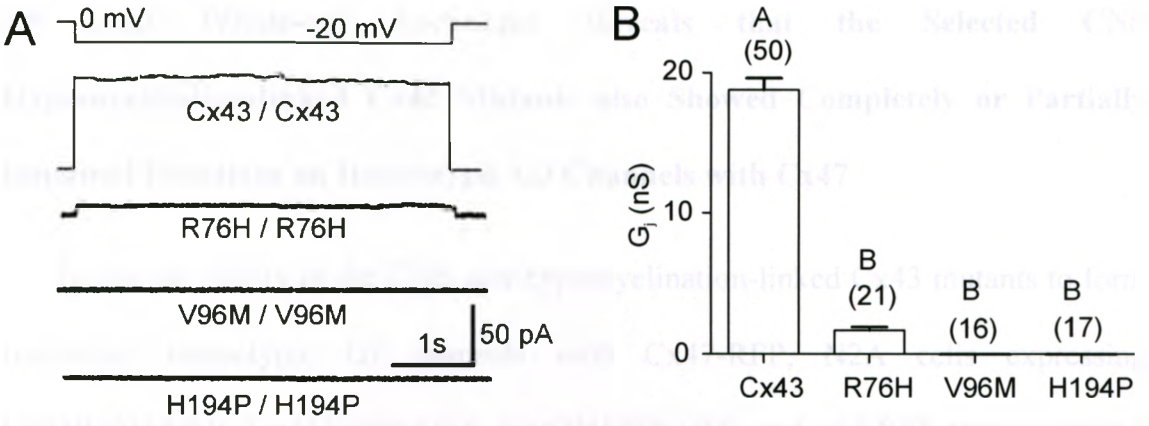

Figure 3-9: Junctional conductance (G_j) measurements between non-hypomyelination-linked Cx43 mutants in the homotypic GJ channel configuration. **(A)** Representative junctional current traces of four homotypic GJ channels illustrate Cx43-GFP, Cx43R76H-GFP, Cx43V96M-GFP or Cx43H194P-GFP in response to a -20 mV voltage step (V_j). N2A cells expressing the Cx43R76H-GFP fusion constructs do form functional homotypic GJ channels in N2A cells with a reduced junctional current. While those cells expressing Cx43V96M-GFP or Cx43H194P-GFP fusion constructs do not. **(B)** The mean G_j of homotypic Cx43-hGFP/ Cx43-GFP = 18.8 ± 0.8 nS (n=50), Cx43R76H-GFP/ Cx43R76H-GFP = 1.7 ± 0.2 nS (n=21), Cx43V96M-GFP/ Cx43V96M-GFP = 0 nS (n=16) and Cx43H194P-GFP/ Cx43H194P-GFP = 0 nS (n=17). A one-way ANOVA with a Tukeys post-hoc test confirmed that there was a significant difference between, Cx43-GFP vs.Cx43R76H-GFP ($p<0.001$), Cx43-GFP vs. Cx43V96M-GFP ($p<0.001$) and Cx43-GFP vs. Cx43H194P-GFP. Significant differences were also found between Cx43R76H-GFP vs. Cx43V96M-GFP ($p<0.001$) and Cx43R76H-GFP vs. Cx43H194P-GFP ($p<0.001$) where significant differences are designated by A vs. B.

3.9 Dual Whole-cell Technique Reveals that the Selected CNS Hypomyelination-linked Cx43 Mutants also Showed Completely or Partially Impaired Functions on Heterotypic GJ Channels with Cx47

To test the ability of the CNS non-hypomyelination-linked Cx43 mutants to form functional heterotypic GJ channels with Cx47-RFP, N2A cells expressing Cx43R76H-GFP, Cx43V96M-GFP, Cx43H194P-GFP or Cx47-RFP were re-plated onto glass coverslips in heterotypic GJ configurations. Representative traces shown in figure 3-10A of Cx43R76H-GFP, Cx43V96M-GFP, and Cx43H194P-GFP paired with Cx47-RFP in heterotypic GJ channel configurations demonstrate the GJ channel function of each pair. It is evident that the Cx43R76H-GFP mutant expressing cells was able to form functional heterotypic GJ channels with Cx47-RFP expressing cells. However, the Cx43V96M-GFP and Cx43H194P-GFP mutants do not form functional heterotypic GJ channels with Cx47-RFP. Figure 3-10B shows the mean G_j of, Cx43-GFP/Cx47-RFP (n=21 from 6 transfections), Cx43R76H-GFP/Cx47-RFP (n=13 from 4 transfections) and Cx43V96M-GFP/Cx47-RFP (n=13 from 3 transfections), and Cx43H194P-GFP/Cx47-RFP (n=12 from 3 transfections). The mean G_j of Cx43R76H-GFP/Cx47-RFP heterotypic GJ channels was found to be 2.1 ± 0.4 nS. In contrast, the mean G_j of both the Cx43V96M-GFP /Cx47-RFP and Cx43H194P-GFP /Cx47-RFP heterotypic GJ channels was found to be 0nS. A one-way ANOVA was performed to compare with a Tukeys post-hoc test. Significant differences were found between each of the following, Cx43-GFP/Cx47-RFP vs. Cx43R76H-GFP/Cx47-RFP ($p<0.05$), Cx43-GFP/Cx47-RFP vs. Cx43V96M-GFP Cx47-RFP ($p<0.001$), Cx43-GFP/Cx47-RFP vs.

Cx43H194P-GFP/Cx47-RFP, Cx43R76H-GFP/Cx47-RFP vs. Cx43V96M-GFP ($p<0.05$) and Cx43R76H-GFP/Cx47-RFP vs. Cx43H194P-GFP/Cx47-RFP ($p<0.05$).

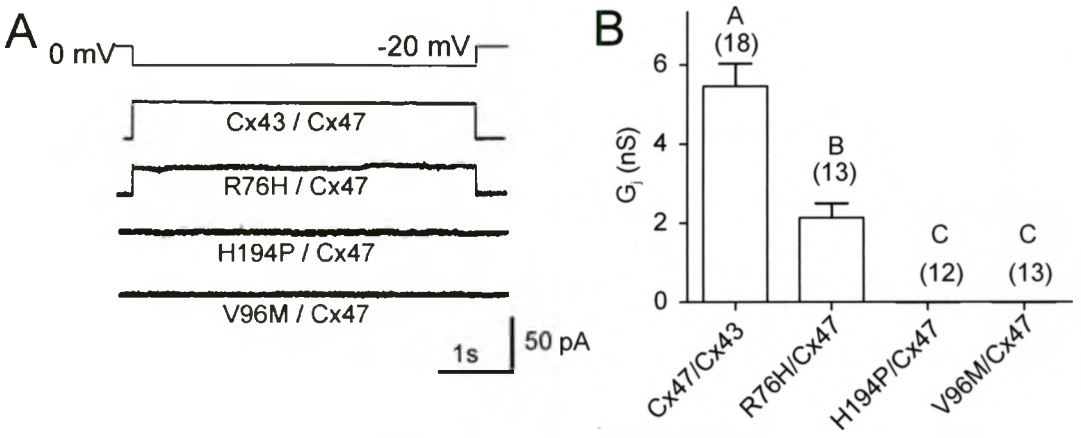

Figure 3-10: Junctional conductance (G_j) measurements between Cx43-GFP non-hypomyelination-linked mutants in the homotypic GJ channel configuration **(A)** N2A cells expressing the Cx43R76H-GFP fusion construct do form a functional heterotypic GJ channel with Cx47-RFP. However, those cells expressing either Cx43V96M-GFP or Cx43H194P-GFP do not form functional heterotypic GJ channels with Cx47-RFP. Representative junctional current traces of four heterotypic GJ channels, Cx43-GFP/Cx47-RFP, Cx43R76H-GFP/Cx47-RFP, Cx43V96M-GFP/Cx47-RFP and Cx43H194P-GFP/Cx47-RFP in response to a -20 mV voltage step (V_j). **(B)** The average G_j of four heterotypic GJ channels is displayed as means, Cx43-GFP/Cx47-RFP = 5.1 ± 0.6 nS (n=18), Cx43R76H-GFP/Cx47-RFP = 2.1 ± 0.4 nS (n=13), Cx43H194P-GFP/Cx47-RFP = 0 nS (n=12), and Cx43V96M-GFP/Cx47-RFP = 0 nS (n=13). A one-way ANOVA with a Tukeys post-hoc test confirmed that there was a significant difference between, Cx43hGFP/Cx47-RFP vs.Cx43R76H-GFP/Cx47-RFP ($p<0.001$), Cx43-GFP/Cx47-RFP vs. Cx43V96M-GFP/Cx47-RFP ($p<0.001$), Cx43-GFP/Cx47-RFP vs. Cx43H194P-GFP /Cx47-RFP ($p<0.05$) and Cx43R76H-GFP /Cx47-RFP vs. Cx43V96M-GFP /Cx47-RFP ($p<0.05$) denoted by A vs. B vs C.

Discussion 4.0

4.1 Overall Scope of Study

The primary goal of this study is to examine the effect of both CNS hypomyelination-linked and non-hypomyelination-linked Cx43 mutations on the function of the Cx43/Cx47 heterotypic GJ channel. It was proposed that Cx43 mutants linked to CNS hypomyelination would cause a disruption of GJIC in the Cx43/Cx47 GJ channel, while CNS non-hypomyelination linked mutants would not. CNS hypomyelination-linked Cx43 mutants (Cx43K134N-GFP, Cx43G138R-GFP, and Cx43V96A-GFP) do not form functional homotypic or heterotypic GJ channels with Cx47-RFP in N2A cells. Interestingly, two of three CNS non-hypomyelination-linked Cx43 mutations, Cx43V96M-GFP and Cx43H194P-GFP do not form functional homotypic or heterotypic GJ channels with Cx47-RFP in N2A cells. The other mutant that is not linked to CNS hypomyelination, Cx43R76H-GFP, is able to form functional homotypic and heterotypic GJ channels with Cx47-RFP in N2A cells, but with a much lower mean G_j in both the homotypic channel and heterotypic configuration with Cx47-RFP in comparison to wild-type Cx43-GFP. This evidence would suggest that both hypomyelination-linked and non- hypomyelination-linked Cx43 mutants cause a disruption in homotypic Cx43 GJIC and in the GJIC of the Cx43/Cx47 GJ channel. Since the Cx43/Cx47 GJ channel is unable to function in our model system it seems reasonable that electrical coupling via the Cx43/Cx47 heterotypic GJ channel is not of great important in the proper maintenance of CNS myelin.

4.2 Distribution of Cx43-GFP

It was important to tag the Cx protein with a fluorescent protein in order to allow for visualization of expression in live cells during dual whole-cell patch clamping technique. More importantly, the use of a GFP and RFP tag allowed us to easily select heterotypic cell pairs during dual whole-cell patch clamp recording. The fusion of GFP at the C-terminal of Cx43 had little effect on the distribution of Cx43 indicating that the biosynthesis, trafficking to cell surface, formation of gap junction plaques and recycling are not changed. The GFP-tag was linked to the C-terminus of Cx43 by a seven amino acid peptide linker. We found that cells transfected with the Cx43-GFP construct were able to express Cx43-GFP and form homotypic GJ plaque-like structures in both N2A and HeLa cells. Clear gap junction plaque-like structures were able to form between two apposing cells or between cells in clusters, with minimal intracellular distribution. It is well known that Cx43 is translated in the ER and trafficked to the Golgi apparatus and finally is brought to the cell membrane, accounting for the intracellular distribution pattern visualized (Jordan et al., 1999). Previous studies have illustrated the ability of Cx43-GFP to form GJ plaque-like structures between N2A, HeLa, and NRK cells with a minimal intracellular distribution. Namely, HeLa Cells expressing either Cx43 or Cx43-GFP were examined in real time and fixed under a confocal microscope. Both the tagged and untagged Cx43 show similar cellular distribution and rapid turnover times, ranging between 2 and 5 hours (Jordan, Solan et al. 1999). Such studies have also compared the expression pattern of both tagged and untagged Cx43, showing no differences (Jordan et al., 1999). Our negative controls (no cDNA or free GFP) did not yield any

GJ plaque-like structures or fluorescence. This data suggests that the Cx43-GFP is able to traffic to the cell membrane and form GJ plaque-like structures in multiple cell types with minimal disturbance created by the addition of the GFP tag.

For the selected ODDD-linked Cx43 mutants we found few differences in the expression and trafficking comparing to those of wildtype Cx43. The Cx43 mutations linked to CNS hypomyelination, Cx43K134N-GFP, Cx43G138R-GFP, and Cx43V96A-GFP were all able to traffic to the cell-cell interface and form GJ plaque-like structures. Previous studies on Cx43G138R-GFP have also shown that this mutant is able to readily traffic to the cell membrane and form GJ plaque-like structures in HeLa and N2A cells (Gong et al., 2005). However, in some instances Cx43K134N-GFP appeared to form more plaque-like structures than that of wild-type Cx43-GFP. The Cx43 mutants not linked to CNS hypomyelination, Cx43R76H-GFP, Cx43V96M-GFP, and Cx43H194P-GFP, were also able to form plaque-like structures between both N2A and HeLa cells. It does not appear that any of the above mutants suffered from any trafficking issues in either N2A or HeLa cells. All transfections were done in parallel with both negative and positive controls. No fluorescence was visualized in the negative control (no cDNA). Conversely, when cells were transfected with the Cx43-GFP construct, they displayed plaque-like structures consistent with previous data. Overall, it appears that all of the ODDD mutants both linked and non-linked to CNS hypomyelination are able to form plaque-like structures between both HeLa and N2A cells.

4.3 Distribution of Cx47-RFP

The results of this study show that the fusion of GFP or RFP to Cx47 had little effect on the distribution of the Cx47 protein, indicating that biosynthesis and trafficking to cell surface formation of gap junction plaques and recycling was not significantly changed. Cx47-GFP demonstrated similar distribution patterns to those previously described, with the ability to form GJ plaques and minimal intracellular localization (Teubner et al., 2001). However, it was evident that tagged Cx47-RFP at the C-terminus did not express at high levels in either N2A or HeLa cells. There are many possibilities as to why Cx47-RFP did not express as well as the other constructs. First, the quality of the construct may have been compromised because of its frequent need to be thawed and frozen, lowering its efficiency. It is possible that the high guanine and cytosine content present in Cx47 mRNA is causing the formation of secondary structures in the RNA, effectively diminishing expression. It is also possible that the 19 amino acid peptide linker region of Cx47-RFP is preventing proper protein folding, resulting in the disruption by the RFP tag. Overall, we were able to obtain workable conditions with little effect on Cx47 trafficking.

4.4 Distribution of Cx43-GFP and Cx47-RFP indicates that colocalization of Cx43 and Cx47 occurs at the cell-cell interface

Our confocal studies indicate that Cx43-GFP and or Cx47-RFP can form green or red GJ plaque-like structures between apposing cell pairs in both HeLa and N2A cells. Additionally, we have also found that Cx43-GFP expressing cells meet and Cx47-RFP expressing cells, co-localizations of green and red fluorescent signals were observed at the cell-cell junctions between two apposing cells in both HeLa and N2A cells. Our results are very similar to the observations of previous studies using α-Cx47 and α-Cx43 antibodies (Orthmann-Murphy et al., 2008). Such, immunofluorescence studies illustrate the co-localizations of red and green fluorescent signals, indicating the formation of plaque-like structures and the allowing identification of heterotypic GJ channels. The two colour system used in this study allowed us to readily identify heterotypic cell pairs during functional analysis.

Cx43 mutants, Cx43K134N-GFP, Cx43G138R-GFP, and Cx43V96A-GFP are able to form homotypic plaque-like structures in both HeLa and N2A cells. It was shown that heterotypic Cx43V96A-GFP/Cx47-RFP may dock and form GJ channels yet, this event was rare and endocytosed vesicular like structures were present. However, it is unclear whether they can effectively form heterotypic plaque-like structures when paired with Cx47-RFP. It is also unclear whether the non-hypomyelination-linked Cx43 mutants, Cx43R76H-GFP, Cx43V96M-GFP, and Cx43H194P-GFP are able to form heterotypic plaque-like structures with Cx47-RFP in either N2A and HeLa cells. Thus, all ODDD linked Cx43 mutants studied appear

to impair the formation of the heterotypic Cx43/Cx47 GJ channel. It has been difficult to properly enhance the expression of Cx47-RFP during transfections, resulting in a weaker overall expression. Higher concentrations of DNA may help to alleviate expression issues and allow for better visualization on the confocal microscope. It is also possible that all Cx43 mutants are partially impaired in docking with Cx47 to a similar degree, leading to the difficulties of identifying plaque-like structures at the cell-cell junctions.

4.5 Homotypic Cx43-GFP GJ Channels and ODDD Mutant Function

Our double patch clamp study indicated that Cx43-GFP is able to form functional homotypic GJ channels. It was previously reported that the fast gate of Cx43 channel is lost when it is tagged with a GFP at the C-terminal (Buskauskas et al., 2001). Cx43-GFP greatly lengthens the transition from the open to closed states for the Cx43-GFP gap junction channel. Our recordings on homotypic Cx43-GFP GJ channels are consistent with this finding and we could not detect steady state within the duration of the voltage steps. Our studies also found that the Cx43-GFP GJ channel did not reach to steady state in response to 30s V_j-voltage steps (± 100 mV). The macroscopic conductance of the Cx43-GFP homotypic GJ channel in N2A cells was large, 18.8 ± 0.8 nS (n=50). Similar levels of Cx43-GFP macroscopic conductance were also documented in HeLa and N2A cells (Buskauskas et al., 2001; Gong et al., 2006). Such data indicates that Cx43-GFP is able to form functional homotypic GJ channels in both HeLa and N2A cells with a characteristic gating profile and a large mean macroscopic conductance.

The ability of CNS hypomyelination-linked and CNS non-hypomyelination-linked Cx43 mutants to form functional GJ channels was largely compromised. All mutants linked to CNS hypomyelination, Cx43K134N-GFP, Cx43G138R-GFP, Cx43V96A-GFP were unable to form functional GJ channels. Such findings are consistent with previous electrophysiological studies conducted on Cx43G138R-GFP and Cx43K134N-GFP, where the number of coupled cells was found to be 0 (Roscoe, Veitch et al. 2005) (Gong, unpublished data). Likewise non- CNS hypomyelination-linked Cx43 mutants, Cx43V96M-GFP and Cx43H194P-GFP were unable to form functional homotypic GJ channels. Of six generated mutants, five of them had a mean macroscopic conductance of 0nS in the homotypic GJ channel configuration. In fact, only one of the mutants, Cx43R76H-GFP was able to form a functional homotypic GJ channel in N2A cells. Nonetheless, the mean macroscopic conductance of Cx43R76H-GFP was markedly reduced 1.7 ± 0.2 nS (n=21), when compared against Cx43-GFP. Microinjection studies validate these findings by showing that Cx43R76H-GFP homotypic GJ channels are able to pass GJ permeable dyes (Lorentz 2010., unpublished data). This suggest that the Cx43R76H-GFP mutation still negatively impacts homotypic Cx43 mediated GJIC. Thus, all mutants generated affect the ability of Cx43 to form functional homotypic GJ channels in N2A cells.

4.6 Homotypic Cx47-RFP GJ Channel Function

Cx47-RFP is able to form functional homotypic GJ channels in N2A cells. Cx47-RFP homotypic channels were found to have a lower mean G_j in comparison to homotypic Cx43-GFP channels. This may be due to the nature of the Cx or the lower

overall expression levels of Cx47-RFP in N2A cells. Moreover, it was found that the Cx47-RFP homotypic channel current decayed rapidly in response to transjunctional voltage steps (up to ±100 mV). The relative sensitivity was similar to both GFP-tagged homotypic Cx47 GJ channels and untagged Cx47 GJ channels (Teubner et al., 2001; Orthmann-Murphy et al., 2007). Also, our preliminary data suggests that the V_j-gating properties and overall macroscopic conductance levels of Cx47-RFP and untagged Cx47 are very similar. This evidence indicates that macroscopic V_j gating properties of the C-terminal GFP or RFP tagged Cx47 are changed substantially from those of untagged Cx47.

4.7 Heterotypic Cx43/Cx47 GJ Channel Function

Our experiments using double patch-clamp recording indicate that Cx43-GFP and Cx47-RFP can form functional GJ channels in N2A cells. The formation of a heterotypic GJ plaque is a rare event in comparison with the formation of homotypic GJ channels. Luckily our two colour-tagging system allows us to visualize colocalizations of green and red fluorescent signals at the cell-cell junctions and cells positive for both were chosen for double patch recording. An asymmetric gating profile was identified in cell pairs expressing Cx43-GFP on one and Cx47-RFP in the other. Our results are very similar to the observations of previous studies using untagged IRES Cx43 and 47 constructs; asymmetric gating was identified via double patch clamp recordings of heterotypic Cx43/Cx47 GJ channels (Orthmann et al., 2008). Moreover, in the heterotypic Cx43/Cx47 GJ configuration, Cx47-RFP remains much more sensitive to mid- to high- level voltage steps than does

Cx43-GFP. It is also important to consider that similar gating profiles were obtained when using both tagged and untagged Cx43 and Cx47 proteins.

Nonetheless, all but one Cx43 ODDD linked mutant investigated in our study was unable to form any heterotypic GJ channels with Cx47-RFP. Revealing that CNS hypomyelination-linked Cx43 mutants, Cx43K134N-GFP, Cx43G138R-GFP, Cx43V96A-GFP and the non-hypomyelination linked Cx43 mutants, Cx43V96M-GFP and Cx43H194P-GFP were unable to form functional GJ channels when paired with Cx47-RFP. Cx43R76H-GFP was able to form functional GJ channels with Cx47-RFP however the mean G_j was significantly reduced to about 1/3 of the wild-type Cx43/Cx47 GJ channel. It is unlikely that the fluorescent tags hindered the ability of Cx43-GFP and Cx47-RFP to form functional channels as the wild-type were able to form functional GJ channels. This data is in opposition with the previously stated hypothesis which states that non-hypomyelination-linked Cx43 mutants will be able to form functional heterotypic GJ channels with Cx47-RFP. It appears that Cx43/Cx47 GJIC is not critical in the maintenance of proper CNS myelination.

4.8 Clinical Features and Implications of Selected Cx43 Mutants

Patients with CNS hypomyelination-linked Cx43 mutations, Cx43K134N-GFP, Cx43G138R-GFP, and Cx43V96A-GFP suffered from overt neurological disorders and abnormalities in CNS myelin (Paznekas et al., 2009; Fenwick et al., 2008). Conversely, patients with Cx43 mutations that displayed CNS non-hypomyelination-linked mutations, Cx43R76H-GFP, Cx43V96M, and Cx43H194P did not show any overt neurological symptoms or CNS myelination abnormalities (Kjaer et al., 2004;

Richardson et al., 2004; Paznekas et al., 2009). Thus, it was predicted that the CNS hypomyelination-linked Cx43 mutants would impair Cx43/Cx47 GJIC where as those Cx43 mutants that are CNS non-hypomyelination-linked would not. It is now clear that both sets of Cx43 mutations negatively impact both homotypic Cx43 GJIC and heterotypic GJIC with Cx47 in N2A cells. Nonetheless, we have found that both sets of human Cx43 mutants impair GJIC with Cx47 indicating that the Cx43/Cx47 GJ channel is not critical in the proper maintenance of CNS myelin. This is the first study to define the function of human Cx43 mutations paired with Cx47.

Several studies have provided insights as to why the Cx43/Cx47 heterotypic GJ channels may not be critical for A/O coupling. It has previously been shown that the Cx32/Cx30 and Cx47/Cx43 GJ heterotypic GJ channels may provide redundant function in terms of A/O GJIC (Maglione, Tress et al. 2010; Magnotti, Goodenough et al. 2010) It is also possible that Cx43 mutants may be acting in a transdominant fashion, inhibiting Cx30 and thus impacting both the Cx43/Cx47 and Cx30/Cx32 heterotypic GJ channels. Previous studies have shown that when co-expressed a Cx can act in a transdominant fashion via heteromeric connexon formation, suppressing GJIC of both Cxs involved. Specifically, various Cx26 mutants Cx26D66H, Cx26R75W, and Cx26W44C when co-expressed with Cx43 result in a 50-95% reduction in coupling via Cx43/Cx43 homotypic GJ channels (Rouan, White et al. 2001). It is also important to consider what effect each mutation has on the hemichannel activity of Cx43. Currently, no data exists on the hemichannel activity of any of the selected Cx43 mutants in this study.

4.9 A/O Coupling is Mediated via Redundant Heterotypic GJ channels - In Vitro Evidence

Multiple human genetic diseases and murine knockout models have illustrated that proper maintenance of CNS myelin is dependent on the proper expression of macroglial Cx's. It is well known that Cx43 and Cx47 play a role in the maintenance of proper CNS myelin function, since mutations in Cx43 or Cx47 have both been associated with CNS myelin abnormalities (Paznekas et al., 2009; Uhlenberg et al., 2004). It was previously stated that oligodendrocytes express Cx29, Cx32, and Cx47 while astrocytes express Cx26, Cx30, and Cx43 where Cx29 and Cx26 are not thought to participate in the formation of GJ channels (Kawasama et al., 2005; Orthmann-Muprhy et al., 2007). Indicating that, A/O coupling via GJIC must be mediated via heterotypic GJ channels. Our study confirms that Cx43 and Cx47 can dock and form functional heterotypic GJ channels in N2A cells. Also, it was found that the Cx43/Cx47 GJ channel exhibited asymmetrical GJ gating in response to voltage steps, consistent with previous electrophysiological data (Orthmann-Murphy et al., 2008). However, it has been proposed that several heterotypic GJ channel configurations can form between A/O. Further, studies using both dye transfer in HeLa cells and electrophysiological recordings on N2A cells have demonstrated that A/O coupling is mediated via the Cx32/Cx30 and the Cx47/Cx43 GJ channels (Orthmann-Murphy et al., 2008). Recently, studies in HeLa cells have even demonstrated that the Cx30/Cx47 heterotypic GJ channel readily passes the dye neurobiotin (Magnotti et al, 2011). Thus, it appears that the Cx43/Cx47, Cx30/Cx32,

and Cx30/Cx47 heterotypic GJ configurations are all theoretically possible and may serve redundant functions with respect to A/O coupling.

4.10 A/O Coupling is mediated via Redundant Heterotypic GJ channels - In Vivo Evidence

One explanation why the disruption of the Cx43/Cx47 GJIC does not result in demyelination is because Cx43/Cx47, Cx32/Cx30, and Cx30/Cx47 GJ channels may have redundant function. Initial studies have demonstrated that Cx32 and Cx47 provide redundant function between single knockout (KO) mice do not show any overt phenotype, yet double KO mice die by the 5^{th} or 6^{th} postnatal week (Scherer et al., 1998; Odermatt et al., 2003; Menichella et al., 2003). Cx43 KO mice are embryonically lethal yet, mice with selective ablation of astrocytic Cx43 do not produce any overt clinical phenotype (Maglione et al., 2010) In concert, studies in murine astrocytes where Cx43 is selectively ablated (Cx43(fl/fl):hGFAP Cre mice) have shown that the loss of Cx43 does not compromise biocytin transfer from oligodendrocytes to astrocytes. (Wallraff et al., 2006; Maglione et al., 2010). Interestingly, it was also found that selective ablation of astrocytic Cx43 did impair the coupling of oligodendrocytes (O/O), restricting biocytin dye transfer to the subpopulation of immature oligodendrocytes (Maglione et al., 2010). Selective ablation of astrocytic Cx43 and Cx30 was made possible by interbreeding Cx43(fl/fl):hGFAP Cre mice with Cx30 deficient mice. Further, A/O coupling in Cx43- and Cx30- double deficient mice is almost completely abolished and O/O coupling is markedly reduced, (Maglione et al., 2010). This may be explained by a compensatory effect of the Cx30/Cx47 channel. In the neocortex of Cx47-null mice

it was shown that A/O coupling was completely abolished, yet in the neocortex of Cx32-null mice A/O was minimally affected (Wasseff and Scherer 2011). Thus, although the Cx32/Cx30 and Cx47/Cx30 channel are thought to serve redundant function it appears that loss of Cx43 alone results in diminished A/O coupling. Our data is in parallel with such studies in that loss of the Cx43 homotypic GJ channel and the Cx43/Cx47 heterotypic GJ channel is insufficient to cause CNS hypomyelination.

4.11 Hemichannel Activity and Apoptosis

Our study compares two mutant sets both of which nearly abolish GJIC between homotypic Cx43 GJ channels and heterotypic Cx43/Cx47 GJ channels. Along with additional evidence it is probable that neither loss of homotypic Cx43 or heterotypic Cx43/Cx47 GJ channels is sufficient to cause CNS hypomyelination. This study may provide insight on why select Cx43 mutations cause hypomyelination while others do not. Another possibility is that the CNS hypomyelination-linked Cx43 mutants will result in an increase in hemichannel activity while the CNS non-hypomyelination-linked Cx43 mutants will not. Up-regulated hemichannel activity and apoptosis have been closely correlated. Specifically certain Cx32 and Cx50 mutants have been associated with increased hemichannel activity, resulting in increased programmed cell death (Minogue et al., 2009; Vinken et al., 2009). ATP release assays were used to determine the activity of Cx32 and Cx50 hemichannels. The results suggested that increases in ATP release was highly correlated with an increase in apoptotic cells (Minogue et al., 2009; Vinken et al., 2009). Thus, it is possible that select Cx43 mutations cause an up-regulation in hemichannel activity,

resulting in an increase of cell death, leading to disruption of both A/A and A/O GJIC which may indirectly affect the viability of oligodendrocytes.

4.12 Conclusion

In summary, these data indicate that impairing heterotypic Cx43/Cx47 GJIC alone is not critical for the maintenance of proper CNS myelin. It was found that both the hypomyelination-linked and non- hypomyelination-linked Cx43 mutants negatively impacted Cx43/Cx47 GJIC in N2A cells. Recent in vitro and in vivo studies support the idea that the loss of Cx43/Cx47 GJIC is compensated for by the redundant Cx30/Cx32 GJ channel and possibly the Cx30/Cx47 GJ channel. This compensation would indicate that A/O GJIC is still critical for the maintenance of regular CNS myelination. However, this explanation does not describe why certain Cx43 mutations cause CNS hypomyelination and others do not. The underlying mechanism connecting certain Cx43 mutants to CNS hypomyelination is possibly due to differences in hemichannel activity. It is also probable that the hypomyelination-linked Cx43 mutants are acting in a transdominant fashion on Cx30. This would cause a disruption in both Cx43/Cx47 and Cx30/Cx32 mediated GJIC, effectively abolishing A/O coupling. Further studies need to be conducted in order to further elucidate the mechanism of Cx dependent CNS hypomyelination.

References

1. Altevogt, B. M., K. A. Kleopa, et al. (2002). "Connexin29 is uniquely distributed within myelinating glial cells of the central and peripheral nervous systems." J Neurosci **22**(15): 6458-6470.

2. Berthoud, V. M., P. J. Minogue, et al. (2004). "Pathways for degradation of connexins and gap junctions." Cardiovasc Res **62**(2): 256-267.

3. Bukauskas, F. F., A. Bukauskiene, et al. (2001). "Gating properties of gap junction channels assembled from connexin43 and connexin43 fused with green fluorescent protein." Biophys J **81**(1): 137-152.

4. Cao, F., R. Eckert, et al. (1998). "A quantitative analysis of connexin-specific permeability differences of gap junctions expressed in HeLa transfectants and Xenopus oocytes." J Cell Sci **111 (Pt 1)**: 31-43.

5. Chalcroft, J. P. and S. Bullivant (1970). "An interpretation of liver cell membrane and junction structure based on observation of freeze-fracture replicas of both sides of the fracture." J Cell Biol **47**(1): 49-60.

6. Das Sarma, J., R. A. Meyer, et al. (2001). "Multimeric connexin interactions prior to the trans-Golgi network." J Cell Sci **114**(Pt 22): 4013-4024.

7. Evans, W. H. and P. E. Martin (2002). "Gap junctions: structure and function (Review)." Mol Membr Biol **19**(2): 121-136.

8. Falk, M. M. (2000). "Connexin-specific distribution within gap junctions revealed in living cells." J Cell Sci **113 (Pt 22)**: 4109-4120.

9. Ferrell, R. E., C. J. Baty, et al. (2010). "GJC2 missense mutations cause human lymphedema." Am J Hum Genet **86**(6): 943-948.

10. Flenniken, A. M., L. R. Osborne, et al. (2005). "A Gja1 missense mutation in a mouse model of oculodentodigital dysplasia." Development **132**(19): 4375-4386.

11. Furshpan, E. J. and D. D. Potter (1957). "Mechanism of nerve-impulse transmission at a crayfish synapse." Nature **180**(4581): 342-343.

12. Furshpan, E. J. and D. D. Potter (1959). "Transmission at the giant motor synapses of the crayfish." J Physiol **145**(2): 289-325.

13. Gilula, N. B. (1987). "Topology of gap junction protein and channel function." Ciba Found Symp **125**: 128-139.

14. Gladwin, A., D. Donnai, et al. (1997). "Localization of a gene for oculodentodigital syndrome to human chromosome 6q22-q24." Hum Mol Genet **6**(1): 123-127.

15. Gong, X. Q., Q. Shao, et al. (2007). "Differential potency of dominant negative connexin43 mutants in oculodentodigital dysplasia." J Biol Chem **282**(26): 19190-19202.

16. Goodenough, D. A., J. A. Goliger, et al. (1996). "Connexins, connexons, and intercellular communication." Annu Rev Biochem **65**: 475-502.

17. Goodenough, D. A. and J. P. Revel (1970). "A fine structural analysis of intercellular junctions in the mouse liver." J Cell Biol **45**(2): 272-290.

18. Jordan, K., J. L. Solan, et al. (1999). "Trafficking, assembly, and function of a connexin43-green fluorescent protein chimera in live mammalian cells." Mol Biol Cell **10**(6): 2033-2050.

19. Kamasawa, N., A. Sik, et al. (2005). "Connexin-47 and connexin-32 in gap junctions of oligodendrocyte somata, myelin sheaths, paranodal loops and Schmidt-Lanterman incisures: implications for ionic homeostasis and potassium siphoning." Neuroscience **136**(1): 65-86.

20. Kjaer, K. W., L. Hansen, et al. (2004). "Novel Connexin 43 (GJA1) mutation causes oculo-dento-digital dysplasia with curly hair." Am J Med Genet A **127A**(2): 152-157.

21. Koval, M. (2006). "Pathways and control of connexin oligomerization." Trends Cell Biol **16**(3): 159-166.

22. Kunzelmann, P., W. Schroder, et al. (1999). "Late onset and increasing expression of the gap junction protein connexin30 in adult murine brain and long-term cultured astrocytes." Glia **25**(2): 111-119.

23. Laird, D. W. (1996). "The life cycle of a connexin: gap junction formation, removal, and degradation." J Bioenerg Biomembr **28**(4): 311-318.

24. Laird, D. W. (2006). "Life cycle of connexins in health and disease." Biochem J **394**(Pt 3): 527-543.

25. Laird, D. W., K. Jordan, et al. (2001). "Expression and imaging of connexin-GFP chimeras in live mammalian cells." Methods Mol Biol **154**: 135-142.

26. Lauf, U., B. N. Giepmans, et al. (2002). "Dynamic trafficking and delivery of connexons to the plasma membrane and accretion to gap junctions in living cells." Proc Natl Acad Sci U S A **99**(16): 10446-10451.

27. Leithe, E. and E. Rivedal (2004). "Ubiquitination and down-regulation of gap junction protein connexin-43 in response to 12-O-tetradecanoylphorbol 13-acetate treatment." J Biol Chem **279**(48): 50089-50096.

28. Li, X., A. V. Ionescu, et al. (2004). "Connexin47, connexin29 and connexin32 co-expression in oligodendrocytes and Cx47 association with zonula occludens-1 (ZO-1) in mouse brain." Neuroscience **126**(3): 611-630.

29. Maeda, S., S. Nakagawa, et al. (2009). "Structure of the connexin 26 gap junction channel at 3.5 A resolution." Nature **458**(7238): 597-602.

30. Maeda, S. and T. Tsukihara (2011). "Structure of the gap junction channel and its implications for its biological functions." Cell Mol Life Sci **68**(7): 1115-1129.

31. Maglione, M., O. Tress, et al. (2010). "Oligodendrocytes in mouse corpus callosum are coupled via gap junction channels formed by connexin47 and connexin32." Glia **58**(9): 1104-1117.

32. Magnotti, L. M., D. A. Goodenough, et al. (2010). "Functional heterotypic interactions between astrocyte and oligodendrocyte connexins." Glia **59**(1): 26-34.

33. Menichella, D. M., D. A. Goodenough, et al. (2003). "Connexins are critical for normal myelination in the CNS." J Neurosci **23**(13): 5963-5973.

34. Menichella, D. M., M. Majdan, et al. (2006). "Genetic and physiological evidence that oligodendrocyte gap junctions contribute to spatial buffering of potassium released during neuronal activity." J Neurosci **26**(43): 10984-10991.

35. Musil, L. S. and D. A. Goodenough (1993). "Multisubunit assembly of an integral plasma membrane channel protein, gap junction connexin43, occurs after exit from the ER." Cell **74**(6): 1065-1077.

36. Nagy, J. I., F. E. Dudek, et al. (2004). "Update on connexins and gap junctions in neurons and glia in the mammalian nervous system." Brain Res Brain Res Rev **47**(1-3): 191-215.

37. Nagy, J. I., A. V. Ionescu, et al. (2003). "Coupling of astrocyte connexins Cx26, Cx30, Cx43 to oligodendrocyte Cx29, Cx32, Cx47: Implications from normal and connexin32 knockout mice." Glia **44**(3): 205-218.

38. Nagy, J. I., X. Li, et al. (2001). "Connexin26 in adult rodent central nervous system: demonstration at astrocytic gap junctions and colocalization with connexin30 and connexin43." J Comp Neurol **441**(4): 302-323.

39. Neher, E., B. Sakmann, et al. (1978). "The extracellular patch clamp: a method for resolving currents through individual open channels in biological membranes." Pflugers Arch **375**(2): 219-228.

40. Odermatt, B., K. Wellershaus, et al. (2003). "Connexin 47 (Cx47)-deficient mice with enhanced green fluorescent protein reporter gene reveal predominant oligodendrocytic expression of Cx47 and display vacuolized myelin in the CNS." J Neurosci **23**(11): 4549-4559.

41. Orthmann-Murphy, J. L., C. K. Abrams, et al. (2008). "Gap junctions couple astrocytes and oligodendrocytes." J Mol Neurosci **35**(1): 101-116.

42. Orthmann-Murphy, J. L., A. D. Enriquez, et al. (2007). "Loss-of-function GJA12/Connexin47 mutations cause Pelizaeus-Merzbacher-like disease." Mol Cell Neurosci **34**(4): 629-641.

43. Orthmann-Murphy, J. L., M. Freidin, et al. (2007). "Two distinct heterotypic channels mediate gap junction coupling between astrocyte and oligodendrocyte connexins." J Neurosci **27**(51): 13949-13957.

44. Orthmann-Murphy, J. L., E. Salsano, et al. (2009). "Hereditary spastic paraplegia is a novel phenotype for GJA12/GJC2 mutations." Brain **132**(Pt 2): 426-438.

45. Paznekas, W. A., S. A. Boyadjiev, et al. (2003). "Connexin 43 (GJA1) mutations cause the pleiotropic phenotype of oculodentodigital dysplasia." Am J Hum Genet **72**(2): 408-418.

46. Paznekas, W. A., B. Karczeski, et al. (2009). "GJA1 mutations, variants, and connexin 43 dysfunction as it relates to the oculodentodigital dysplasia phenotype." Hum Mutat **30**(5): 724-733.

47. Pizzuti, A., E. Flex, et al. (2004). "A homozygous GJA1 gene mutation causes a Hallermann-Streiff/ODDD spectrum phenotype." Hum Mutat **23**(3): 286.

48. Rackauskas, M., M. M. Kreuzberg, et al. (2007). "Gating properties of heterotypic gap junction channels formed of connexins 40, 43, and 45." Biophys J **92**(6): 1952-1965.

49. Rackauskas, M., V. K. Verselis, et al. (2007). "Permeability of homotypic and heterotypic gap junction channels formed of cardiac connexins mCx30.2, Cx40, Cx43, and Cx45." Am J Physiol Heart Circ Physiol **293**(3): H1729-1736.

50. Rash, J. E., T. Yasumura, et al. (2001). "Identification of cells expressing Cx43, Cx30, Cx26, Cx32 and Cx36 in gap junctions of rat brain and spinal cord." Cell Commun Adhes **8**(4-6): 315-320.

51. Revel, J. P. and M. J. Karnovsky (1967). "Hexagonal array of subunits in intercellular junctions of the mouse heart and liver." J Cell Biol **33**(3): C7-C12.

52. Rook, M. B., H. J. Jongsma, et al. (1988). "Properties of single gap junctional channels between isolated neonatal rat heart cells." Am J Physiol **255**(4 Pt 2): H770-782.

53. Roscoe, W., G. I. Veitch, et al. (2005). "Oculodentodigital dysplasia-causing connexin43 mutants are non-functional and exhibit dominant effects on wild-type connexin43." J Biol Chem **280**(12): 11458-11466.

54. Rouach, N., E. Avignone, et al. (2002). "Gap junctions and connexin expression in the normal and pathological central nervous system." Biol Cell **94**(7-8): 457-475.

55. Rouan, F., T. W. White, et al. (2001). "trans-dominant inhibition of connexin-43 by mutant connexin-26: implications for dominant connexin disorders affecting epidermal differentiation." J Cell Sci **114**(Pt 11): 2105-2113.

56. Sasaki, T. and P. R. Garant (1986). "Fate of annular gap junctions in the papillary cells of the enamel organ in the rat incisor." Cell Tissue Res **246**(3): 523-530.

57. Scherer, S. S., Y. T. Xu, et al. (1998). "Connexin32-null mice develop demyelinating peripheral neuropathy." Glia **24**(1): 8-20.

58. Severs, N. J., K. S. Shovel, et al. (1989). "Fate of gap junctions in isolated adult mammalian cardiomyocytes." Circ Res **65**(1): 22-42.

59. Sosinsky, G. (1995). "Mixing of connexins in gap junction membrane channels." Proc Natl Acad Sci U S A **92**(20): 9210-9214.

60. Thomas, T., K. Jordan, et al. (2005). "Mechanisms of Cx43 and Cx26 transport to the plasma membrane and gap junction regeneration." J Cell Sci **118**(Pt 19): 4451-4462.

61. Uhlenberg, B., M. Schuelke, et al. (2004). "Mutations in the gene encoding gap junction protein alpha 12 (connexin 46.6) cause Pelizaeus-Merzbacher-like disease." Am J Hum Genet **75**(2): 251-260.

62. Vitiello, C., P. D'Adamo, et al. (2005). "A novel GJA1 mutation causes oculodentodigital dysplasia without syndactyly." Am J Med Genet A **133A**(1): 58-60.

63. Wasseff, S. K. and S. S. Scherer (2011). "Cx32 and Cx47 mediate oligodendrocyte:astrocyte and oligodendrocyte:oligodendrocyte gap junction coupling." Neurobiol Dis **42**(3): 506-513.

64. White, T. W., D. L. Paul, et al. (1995). "Functional analysis of selective interactions among rodent connexins." Mol Biol Cell **6**(4): 459-470.

65. Willecke, K., J. Eiberger, et al. (2002). "Structural and functional diversity of connexin genes in the mouse and human genome." Biol Chem **383**(5): 725-737.

66. Xin, L., X. Q. Gong, et al. (2011). "The role of amino terminus of mouse Cx50 in determining transjunctional voltage-dependent gating and unitary conductance." Biophys J **99**(7): 2077-2086.